

BUILDING A 25MHz NMR SPECTROMETER

MAXIMILIAN STABEL

born on 03.11.1995
citizen of Germany

A thesis submitted to attain the degree of
Master of Science ETH in Electrical Engineering and Information Technology
(MSc ETH EEIT)

ETH zürich

examined by

Prof. Roland Riek
Prof. Sebastian Kozerke

supervised by

Dr. Takuya Segawa

2023-09-30

Name ETH_Zurich-Master_Thesis-Maximilian_Stabel
Compiled on 2023-09-30 22:48:28+02:00
 ◆ 8837813 (master)
Engine LuaHBTeX, Version 1.15.0 (TeX Live 2022/CVE-2023-32700 patched)
L^AT_EX Version L^AT_EX 2_E (2022-06-01)
Glossary makeglossaries
Bibliography biblatex + biber
Generator latexmk
Class 2022/10/12 v3.38 KOMA-Script + kaobook
Font TeXGyrePagella, Sans: MerriweatherSans, Mono: Inconsolatazi
Math Font TeXGyrePagellaMath, Operators: cmmi
Font Size 10.95pt

*I may not have gone where I intended to go,
but I think I have ended up where I needed to be.*
— Douglas Adams

This page intentionally left blank.

ABSTRACT

Nuclear Magnetic Resonance spectroscopy (NMR) is a widely used analytical technique in various fields including drug discovery, structural analysis and quality control. Financial hurdles prevent the Global South from profiting from this tool — a limiting factor in medicine, chemistry and physics research. This thesis describes the design, characterization, construction and usage of an open-source low-cost low-field easy-to-build portable NMR spectrometer from off-the-shelf and readily available electronic components capable of spectroscopic measurements. Care has been taken to use inexpensive parts (≈ 9 kCHF magnet, ≈ 1 kCHF electronics), open-source software and tools available in most workshops. Controlled through a simple cross-platform Python package it is easily extensible and modifiable. It provides a starting point for further development and contributes to the efforts of providing easy access to NMR technologies worldwide.

This page intentionally left blank.

CONTENTS

ABSTRACT	v
CONTENTS	vii
1 INTRODUCTION	1
2 NMR CONCEPTS	3
3 THE SPECTROMETER	7
3.1 The console	9
3.2 The power amplifier	13
3.3 The switch	16
3.4 The probe	19
3.5 The low noise amplifier	24
3.6 The 32-channel current source	26
3.7 The magnet	29
3.8 The software	30
4 THE COMPLETE SPECTROMETER	31
4.1 Software Setup	31
4.2 Setting up the RedPitaya	32
4.3 Setting up the control software	33
4.4 Performing a Measurement	34
4.5 Editing the control software	36
5 EXPERIMENTAL RESULTS	37
5.1 Measuring a water signal	37
5.2 Measuring a Toluene signal	44
6 CONCLUSION	47
APPENDIX	49
A SCHEMATICS	51
A.1 The power amplifier	51
A.2 The switch	52
A.3 The low noise amplifier	53
A.4 The 32-channel current source	54
A.5 The magnet	57
B LISTS OF PARTS	59
B.1 The power amplifier	60

B.2 The switch	61
B.3 The low noise amplifier	62
B.4 The 32-channel current source	63
BIBLIOGRAPHY	65
LIST OF TERMS	69
DECLARATION OF ORIGINALITY	73

LIST OF FIGURES

1.1 "NMR publications" per million capita (2021). Countries coloured in white have no access to NMR, while Switzerland appears as a global leader in NMR science. (Dr. Maria Pechlaner, Infozentrum Chem. Biol. Pharm., ETH Zürich; database: Scopus)	2
2.1 A rectangle window function of length 1 s in time domain with an amplitude of 1 on the left side and its Fourier transform on the right side, capped to ± 10 Hz	5
2.2 An infinite sine wave of 20 Hz plotted from -1 s to 1 s on the left side and its Fourier Transform on the right	5
2.3 A pulsed sine wave of 20 Hz and a pulse length of 1 s plotted from -1 s to 1 s on the left side and its Fourier Transform on the right. Notice the broadening in the centre compared to the pure sine wave in Figure 2.2. We are sending multiple frequencies around 20 Hz at the same time simply by pulsing a single frequency sine wave.	6
3.1 Block Diagram. The main components of the <i>magnETHical</i> NMR spectrometer, include the console, lowpass filters, analogue amplifiers, transmit-receive switch and transmit-receive coil.	8
3.2 RedPiaya SDRlab 122-16. 3D rendering of the console in KiCAD. Can be thought of as an "RF Raspberry Pi". It has a Dual Core ARM Cortex A9, 512 MB RAM, Gigabit Ethernet, 2x transmit, 2x receive, an ADC sample rate of 122.88 MS/s, 16 bit resolution, a bandwidth of 300 kHz to 550 MHz and a voltage range of $0.5 \text{ V}_{\text{pp}} / -2 \text{ dBm}$ (50Ω). The DAC has the same sample rate and voltage range, but a resolution of 14 bit and a bandwidth of 300 kHz to 60 MHz.	10
3.3 MaRCoS system architecture. "The server receives a sequence from the client PC via Ethernet and streams it to the FPGA firmware, where it is translated into time-synchronous hardware operations including RF and gradient outputs. The firmware receives data from the ADCs, demodulates and filters it, and saves it into RX buffers, from which it is read by the server and sent to the PC" ([12], Figure 3) Magnetic field gradients are not necessary for spectroscopy and thus not used.	11
3.4 Receive input protection of crossed shunt BYS10 Schottky diodes attenuating the signal. The attenuation is unacceptably high. The input signal of $100 \text{ mV}_{\text{pp}}$ is attenuated down to $24 \text{ mV}_{\text{pp}}$ or by about 12 dB.	12
3.5 Working receive input protection of crossed shunt RB520SM-30 Schottky diodes. The Schottky diodes attenuate the 500 mV input signal to about 426 mV, equivalent to a power attenuation of 1.4 dB.	13
3.6 RF power amplifier. 3D rendering of the power amplifier PCB in KiCAD. The signal travels from left to right with the power supply circuitry above. It contains two MMIC amplifier stages, the AD5536 and the PHA-202+. A -6 dB attenuator was added in between and a passive low-pass filter in front ($f_c = 35 \text{ MHz}$). $G \approx 32 \text{ dB}$, $P_{1 \text{ dB}} \approx 30 \text{ dBm}$	15

3.7	The passive switch. Based on Diodes and RF properties, the passive switch forwards the signal based on signal power. Due to the diode characteristics, the switch leaks up to 0.7 V without attenuation — including noise.	17
3.8	Passive RF T/R switch The power amplifier output would be connected on the left, the probe at the top and the low noise amplifier on the right.	17
3.9	RFT/R switch 3D rendering of the switch PCB in KiCAD. The transmit and receive amplifiers are connected on the left and right, the probe at the bottom connector. The central part is a Qorvo QPC6324 Single Pole, Double Throw (SPDT) switch. Above it is a linear power supply and connection pins for active switching and power supply.	19
3.10	Manufacturer's probe holder and RF coil with tuning and matching capacitors The body was 3D printed and the circuit cut by hand.	20
3.11	The S_{11} coefficient of the manufacturer probe On an x-scale from 20 to 30 MHz and a logarithmic y-scale in dB. Measured with a Rhode & Schwarz ZNB 4 VNA.	21
3.12	Probe holder and RF coil with tuning and matching capacitors The capacitors are tunable from 4.5 to 20 pF of make JZ200HV. The coil has a diameter of $d = 7.5$ mm, wire diameter $D = 0.2$ mm and $n = 18$ turns on a length of $l = 4$ mm. It has a measured inductance of $L_{1\text{MHz}} = 2.7 \mu\text{H}$ and a resistance of $R_{1\text{MHz}} = 0.63 \Omega$. The body was 3D printed and the circuit cut by hand.	22
3.13	The S_{11} coefficient of the home-built probe On an x-scale from 20 to 30 MHz and a logarithmic y-scale in dB. Measured with a Rhode & Schwarz ZNB 4 VNA.	23
3.14	The low noise amplifier 3D rendering of the low noise amplifier PCB in KiCAD. The signal travels from left to right through a low-pass filter with 1.8 GHz cut-off frequency, a 5 dBm clamping diode and the PHA-13LN+ low noise amplifier ($G = 24$ dB, $N = 1$ dB, $P_{1\text{dB}} = 23$ dBm @20 MHz). The power is supplied by the onboard linear regulator at the top	24
3.15	VNA S_{11} and S_{21} measurement. An S_{11} of -14.47 dB and a S_{21} of 23.21 dB was measured at 25 MHz using a nanoVNA-H4.	25
3.16	Amplifier concatenation test. Oscilloscope measurement of a function generator signal of $10 \text{ mV}_{\text{pp}} / -36 \text{ dBm}$ attenuated by 30 dB ($= -66 \text{ dBm}$) that was amplified by three low noise amplifiers built here separated by two 3 dB attenuators and a low pass filter ($S_{21} < 0.3$ dB) at the end. Expected total amplification is thus $G \approx 63.3$ dB. Measured -2 dBm equivalent to the full console input range, giving an amplification of 64 dB.	26
3.17	Active electronic shim system. The shown system was pre-installed inside the dipole magnet. The bottom side is shown, the top side is the equivalent. Current is supplied through the connectors at the bottom, each vertical pair connected to one shim.	27
3.18	Simulation schematic of one channel of the current source in LTSpice. The output voltage of the AD5676R is in practice set through SPI by the console. It is important to not set the supply voltage too high, because excess voltage will drop over the OpAmp generating heat.	27

3.19	Simulation result of one current source channel. The dashed blue line is the resulting output current set by the output voltage of the DAC shown in solid orange. The curves deviate slightly, but this can be later corrected in software. Schematic of the simulation can be found in Figure 3.18. Simulated using LTSpice.	28
3.20	32-channel programmable current source. 3D rendering of the current source PCB in KiCAD. The SPI interface is on the right, the power connectors on the left and the 32 output channels on the top and bottom of the PCB. It consists of 4 8-channel ADCs (AD5676R) setting a voltage that is converted to a constant current by two OpAmps: LMV358 for signal scaling and shifting and TCA0372 for the constant current source.	28
3.21	Alternative current source channel schematic. This push-pull circuit has higher current drive capabilities through the use of FET output stages. The zero point is compensated by the third OpAmp reducing quiescent currents compared to a resistor divider. Simulated in LTSpice, taken from [9] (page 778, chapter 11.3.3.1)	29
4.1	Logo of the <i>magnETHical</i> spectrometer project	31
4.2	Component overview. The schematic contains all physical parts of the NMR spectrometer that need to be connected through SMA cables.	32
5.1	Simple pulse sequence The usual depiction of a simple pulse sequence. The “RF pulse” is a high frequency RF pulse close to the resonance frequency of the nuclei to be observed. After the pulse, a decaying cosine signal can be received on the same coil - the so-called Free Induction Decay (FID).	37
5.2	Free Induction Decay (FID) of water. The signal was recorded after a $8\ \mu\text{s}$ impulse of a strength of 1 W and a delay of $25\ \mu\text{s}$, waiting for the coil to ring down. “Andrew’s probe” was used in this measurement with a transmit frequency of 25.09 MHz	37
5.3	Free Induction Decay (FID) of water with a sine fit. The blue data is the same as in Figure 5.2. The orange dashed line is the result of a least squares fit of a decaying sine wave. It shows an exponential decay in amplitude with a T_2^* of 2.5 ms and a dominant frequency of about 590 Hz	38
5.4	Structure of H_2O. Observe the two H atoms that should result in an identical NMR signal.	38
5.5	Fourier spectrum of Figure 5.2. It shows a Lorentz-shaped peak around roughly 600 Hz with a slight broadening on the right side and a distorted baseline. The data was obtained through an automatic zero fill, complex Fourier transformed and automatically zero order phase corrected with a shift of 37°	39
5.6	Fourier spectrum of Figure 5.2 with lorentzian fit. The Lorentzian curve was fit using a least-squares minimization approach. It is centred around $-576\ \text{Hz}$ with a full width at half maximum of 118 Hz resulting in a T_2^* of 2.7 ms.	40
5.7	Rabi nutation of the water signal. Each data point was generated by performing an FID experiment as described in Figure 5.2 and integrating over the resulting peak (see Figure 5.5) to obtain a measure of signal strength. The zero-order phase correction applied to all points was identical.	41

5.8	Rabi nutation of the water signal with decaying sinus fit. The data was fit using a least-squares approach to fit a decaying sinusoidal function. The fit has a period of $32 \mu\text{s}$, giving the length of a $\frac{\pi}{2}$ -pulse of $8 \mu\text{s}$	41
5.9	Spin echo sequence. A possible depiction of the spin echo sequence. A pulse of a duration that causes a $\frac{\pi}{2}$ rotation of the spins and a pulse twice as long (i.e. length π) are applied with a delay of duration τ in between. A spin echo is then observed with its peak after a delay of τ after the second pulse.	41
5.10	Spin Echo. Measurement of the received signal after the last pulse of a classic spin echo sequence (see Figure 5.9). The $\frac{\pi}{2}$ of $9 \mu\text{s}$ was sent with a power of 1 W. The delay between pulses τ was 100 ms. Data was recorded for 130 ms after the last pulse.	42
5.11	Le Petit Prince. "My drawing was not a picture of a hat. It was a picture of a boa constrictor digesting an elephant." — Antoine de Saint-Exupéry	42
5.12	Fourier Transform of decaying spin echoes over delay length τ. The phase-corrected Fourier transforms are plotted in three dimensions over the delay τ in between the pulses. The decay of the signal strength with increasing delay is clearly visible.	43
5.13	T_2 decay of water. Each data point is obtained by integrating the peak of the phase-corrected Fourier spectrum of a spin echo experiment as seen in Figure 5.12. One can vaguely discern the expected exponential decay.	43
5.14	T_2 decay of water with an exponentially decaying function fitted. The data points are the same as in Figure 5.13. The least-squares fit has a T_2 decay time of 190 ms.	44
5.15	Chemical structure of Toluene. Notice the two main components: The CH_3 methyl group on one side and the phenyl ring on the other. The hydrogen atoms in both have very distinct NMR resonance frequencies and differ by about 5 ppm.	44
5.16	FID of Toluene. It was recorded under similar conditions as the water above. A simple $\frac{\pi}{2}$ -pulse of $9 \mu\text{s}$ with 1 W power at 25.0904 MHz was sent. After a delay of $25 \mu\text{s}$ the signal was recorded for 20 ms.	44
5.17	FFT of Toluene measurement and simulation over a ppm scale. The blue data line was obtained through a Fourier transformation of the signal in Figure 5.16. It was manually shifted by 170 Hz as there is no locking yet. The orange signal was created using MestReNova 14.3.3 simulating a spectra of Toluene at a B_0 field of 25 MHz, a peak width of 50 Hz and scaled to match the measurement scale.	45

LIST OF TABLES

3.1	Comparison of different NMR spectrometer types. Prices are estimates based on previous purchases of the lab and experience in the price developments across vendors.	8
-----	---	---

3.2 Prices of the individual parts of the built spectrometer in comparison. Prices include VAT in CHF	9
---	---

LIST OF LISTINGS

1 Generating SSH keyfiles for passwordless login. Accept default configurations when prompted.	33
2 Installing prerequisites	33
3 Set up of a “virtual environment” (often called “venv”) in Python	34
4 Installation of the python library with automated dependency resolution using pip. Assuming the user already installed and activated a virtual environment as described in Listing 3.	34
5 Command line spectrometer control commands	34
6 Performing a measurement on a sample using the control software. The hardware is assumed to be set up, connected and powered up. The 5 mm NMR tube with the sample should be inside the probe holder that was inserted into the magnet and the connection between the RedPitaya and the Laptop running the control software was verified. The code sends a single pulse of 9 μ s, waits for 25 μ s, records the received signal and plots it in the time and frequency domains.	35
7 Using hatch to perform common tasks when editing the control software. The invoked commands can be found in the <code>pyprojects.toml</code> file in the repository. Examples for using the library are available in the <code>scripts</code> and <code>docs</code> folders.	36

This page intentionally left blank.

INTRODUCTION

1

Aller Anfang ist schwer.

— German Proverb

In 1896 the Dutch physicist Pieter Zeemann discovered that the visible spectral lines of a mercury vapour lamp split up in the presence of a magnetic field [1]. In 1938 Isidor Rabi then first described nuclear Magnetic Resonance (MR) [2]. His technique was in turn extended by Felix Bloch [3] and Edward Mills Purcell [4] and is nowadays one of the most powerful tools in analytical sciences. It can be used for analysing the structure of molecular systems, studying crystals and imaging in medicine among others. In 1966 Richard Robert Ernst developed Fourier Transform Nuclear Magnetic Resonance spectroscopy (FT-NMR) [5], which is the same fundamental technique still used today.

Since then, the technology has advanced fast to higher magnetic field strengths and higher processing power. Enabling better images, higher resolutions and new technology magnetic resonance has become an essential part of many scientists' toolboxes. Unfortunately, higher capabilities come hand in hand with higher costs.

Not much effort has gone towards using the technological advancements of recent decades to lower the cost of magnetic resonance technology. Therefore, there are myriads of lost opportunities in education, industry and research. The global south is disproportionately affected by this trend. This can be seen easily when looking at the number of NMR publications published in a given country in Figure 1.1. This is in line with the growing disparity in citations [6].

NMR is used across various fields, making the lack of NMR specialists in the Global South a dire problem. It is used in research — as an example — for chemical, physical and structural analysis and drug discovery. It is used in medicine for non-invasive imaging with the famous MRI machine, in industry for process control in the petroleum industry or drug screening and in education to teach concepts of NMR, quantum mechanics and even fundamentals of quantum computing. The lack of NMR technology thus affects a broad range of fields.

[1]: Zeeman (1896), *On the Influence of Magnetism on the Nature of the Light Emitted by a Substance*.

[2]: Rabi *et al.* (1938), *A New Method of Measuring Nuclear Magnetic Moment*

[3]: Bloch *et al.* (1946), *The Nuclear Induction Experiment*

[4]: Purcell *et al.* (1946), *Resonance Absorption by Nuclear Magnetic Moments in a Solid*

[5]: Ernst *et al.* (1966), *Application of Fourier Transform Spectroscopy to Magnetic Resonance*

[6]: Nielsen *et al.* (2021), *Global Citation Inequality Is on the Rise*

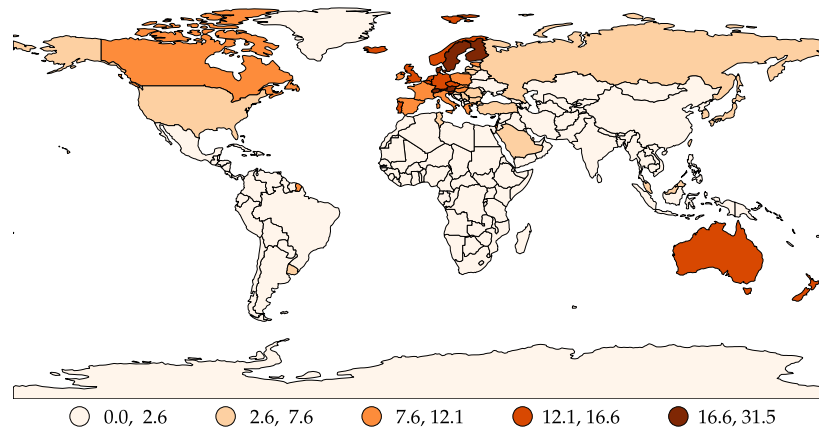


Figure 1.1: “NMR publications” per million capita (2021). Countries coloured in white have no access to NMR, while Switzerland appears as a global leader in NMR science. (Dr. Maria Pechlaner, Innozentrum Chem. Biol. Pharm., ETH Zürich; database: Scopus)

1: The full documentation including the source codes is currently available at the [official Git repository](https://github.com/M4a1x/nmr-spectrometer) (<https://github.com/M4a1x/nmr-spectrometer>)

To tackle this problem, the presented work focuses on lowering the entry barrier to magnetic resonance research, specifically **Nuclear Magnetic Resonance spectroscopy (NMR)**. Consequently, we developed a low-cost easy-to-use easy-to-build low-field **NMR** spectrometer. The detailed, hands-on documentation includes specifications, simulations, full hardware descriptions, CAD designs Python control code and reproducible measurement results¹.

First, the general concept of an **NMR** spectrometer is briefly introduced in [Chapter 2](#), which is then expanded upon in detail when describing the individual parts of the built spectrometer in [Chapter 3](#). Having delved into all the parts of an **NMR** spectrometer [Chapter 4](#) describes the usage of the whole system. [Chapter 5](#) then presents the measurement results obtained with the built spectrometer. Finally, [Chapter 6](#) ends with a conclusion and the high-level achievements of this work together with an outlook of still-to-be-done tasks.

NMR CONCEPTS

2

*You can never be
overdressed or overeducated.*

— Oscar Wilde

This chapter will quickly introduce the topics an inclined reader with an electronics background might need a short introduction to. It aims to be a quick reminder of the most important formulas and concepts without going into any depth. A full introduction to chemistry and **NMR** is outside the scope of this text. For a better introduction than the author will ever be capable of, please take a look at other literature, such as “Spin Dynamics”[7], “Experimental Pulse NMR”[8] for the chemistry and “Halbleiter-Schaltungstechnik”[9] or “The Art of Electronics”[10] for the electrical engineering.

Simply put, a nucleus of an “NMR active” atom will absorb and then later emit radio waves at a specific frequency that depends on an external magnetic field – the stronger the field the higher the frequency:

$$\omega = -\gamma B_0$$

The specific frequency ω is usually called the *Larmor frequency*. γ is called the *gyromagnetic ratio* and depends on the atom. Finally, B_0 is the name for the external static magnetic field produced by a large magnet¹.

The magnetic dipole moment $\vec{\mu}$ can be but in relation with the quantum spin number \vec{S} through the same gyromagnetic ratio γ

$$\vec{\mu} = \gamma \vec{S}$$

This tells us that atomic nuclei with both an even number of protons and neutrons do not show this effect, because their spin is zero and thus have no nuclear magnetic dipole moment, which can be easily verified with the equation above. Examples of nuclei that are so-called “NMR active” include ¹H, ¹³C and ¹⁹F among others.

Nature now has it, that the exact frequency that the nuclei *resonante* with depends on their surroundings. Inversely, we can thus exploit this property to figure out these surroundings if we know the frequency at which the nuclei resonate.

[7]: Levitt (2008), *Spin Dynamics: Basics of Nuclear Magnetic Resonance*

[8]: Fukushima (1981), *Experimental Pulse NMR: A Nuts and Bolts Approach*

[9]: Tietze *et al.* (2019), *Halbleiter-Schaltungstechnik*

[10]: Horowitz *et al.* (2022), *The Art of Electronics*

1: As opposed to B_1 which is the magnetic component of the field generated by an **RF** pulse.

Surroundings include for example whether an atom is located next to another atom not only in space due to some folding of a long molecule, but also whether a chemical bond is present as well.

Thus we need to send radio waves at multiple frequencies and then look at the corresponding return signals recording the different resonant frequencies and amplitudes. From these measured shifts of the expected resonance frequency to the observed scientists can perform structural, chemical and physical analysis. Chemists usually specify the resonance frequency relative to a reference resonance frequency, that is by international convention [TMS](#). To speed this process up, we can send all frequencies we're interested in at the same time using so-called [FT-NMR](#).

Placed inside an external magnetic field we call B_0 and excited with the right frequency radio wave the total spin magnetization will start precessing around the external magnetic field B_0 according to the relation

$$\omega = -\gamma B_0$$

where γ is again the gyromagnetic ratio and $\omega = 2\pi f$ with f being the precession frequency. This precession can be observed when the excitation radio wave stops and we listen for radio waves emitted by the nuclei as they relax from their excited state back to their previous state. Because the resonant frequency is also dependent on the surroundings² of the atom, structural, chemical and physical analysis can be performed by measuring this shift of expected resonance frequency to the observed. Chemists call this shift in frequency the "Chemical Shift (CS)".

2: For example couplings inside the molecule

3: In practice just *very* long

4: In practice, a specific algorithm called Fast Fourier Transform (FFT) is used. If it is performed on discrete values (e.g. arrays of data), it is often called DFFT for Discrete Fast Fourier Transform

The conceptually simplest method of NMR spectroscopy would be to send an "infinitely" long³ radio wave with a slowly changing frequency to find the exact frequencies that the nuclei resonate at. This technique is called [Continuous Wave Nuclear Magnetic Resonance spectroscopy](#) or short [CW-NMR](#).

The Fourier theorem states that any periodic signal can be written as a sum of pure sinus waves. In practice, any time signal can be viewed as periodic with a period of infinity. The process of decomposing a signal into its sine components is called Fourier Transform (FT)⁴. The other way around — composing a signal by summing up pure sine waves — is called inverse Fourier Transform or iFT.

The concept of Fourier Transformation can then be used to very easily send multiple frequencies at once. This concept is called

pulsed NMR or FT-NMR. The simplest pulse is a multiplication of a rectangle signal (see the left side of [Figure 2.1](#)) with a simple pure sine wave (see the left side of [Figure 2.2](#)) with a frequency close to the suspected resonance frequency. In practice, this simply means quickly switching the transmission of the sine wave on and off (see the left side of [Figure 2.3](#)). Because a single rectangle pulse consists of many frequencies (right side of [Figure 2.1](#)), only a single pulse of a sine wave close to the relevant resonant frequency is needed to excite multiple nuclei with slightly different resonance frequencies (see [Figure 2.2](#) and [Figure 2.3](#))⁵. The shorter the pulse, the more frequencies can be excited, but less energy is transmitted in total and per frequency.

5: A multiplication of the time domain signals results in a convolution in the frequency domain

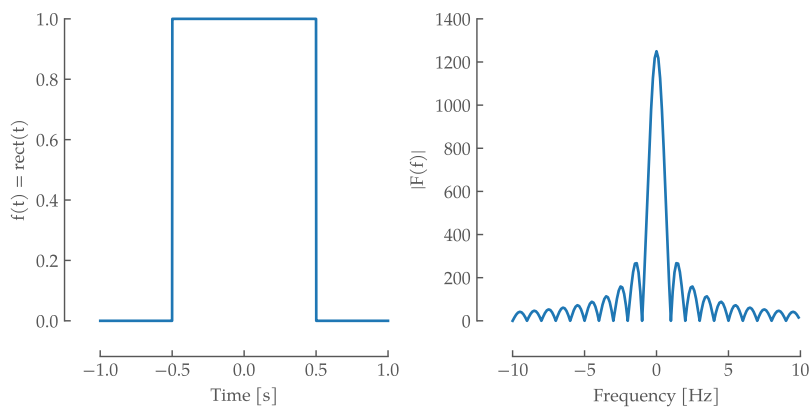


Figure 2.1: A rectangle window function of length 1 s in time domain with an amplitude of 1 on the left side and its Fourier transform on the right side, capped to ± 10 Hz

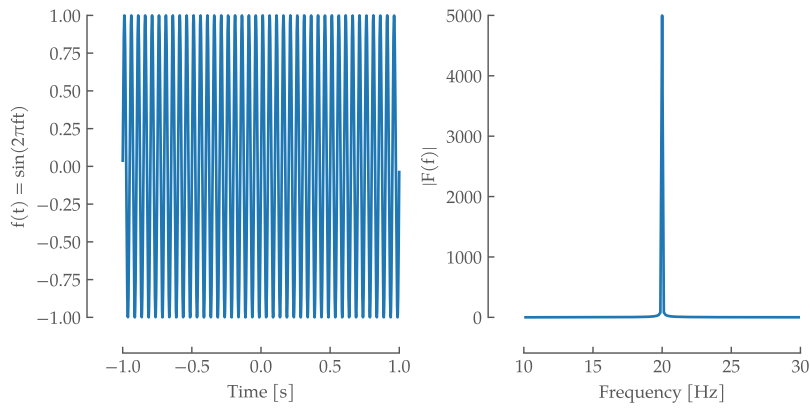


Figure 2.2: An infinite sine wave of 20 Hz plotted from -1 s to 1 s on the left side and its Fourier Transform on the right

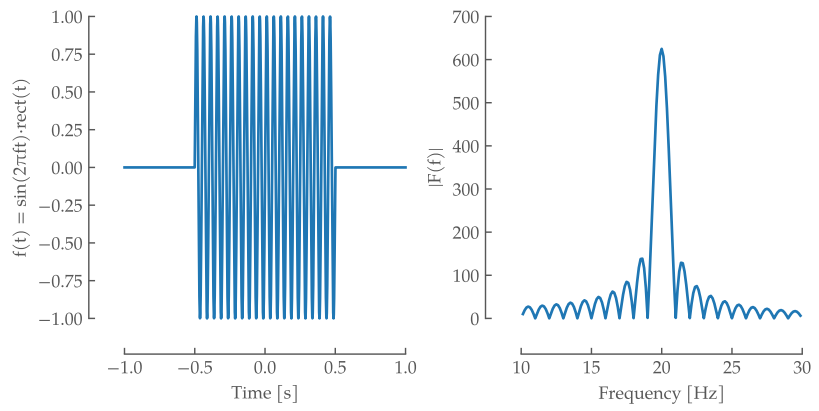


Figure 2.3: A pulsed sine wave of 20 Hz and a pulse length of 1 s plotted from -1 s to 1 s on the left side and its Fourier Transform on the right. Notice the broadening in the centre compared to the pure sine wave in [Figure 2.2](#). We are sending multiple frequencies around 20 Hz at the same time simply by pulsing a single frequency sine wave.

THE SPECTROMETER

3

*What I cannot create,
I do not understand.*

— Richard Feynman

The individual parts of the spectrometer have been designed with several goals in mind. The main guiding principle was reproducibility and availability such that anyone can reproduce the build with minimal effort. All the necessary steps are documented below, including the reasoning for steps not taken. For verification and testing of the parts below the console (see [Section 3.1](#)) itself may be used¹. A more practical solution is using separate devices for this to avoid the reconfiguration hassles. The open-source NanoVNA-H4² [VNA](#) and the tinySA³ spectrum analyser are affordable and at these frequencies very capable alternatives to expensive lab equipment. They have been used extensively during the development of the hardware.

The following sections describe the design and build process — including the reasoning behind the decisions taken — of the *magnETHical* NMR spectrometer. [Figure 3.1](#) shows an overview schematic of the main components that will be discussed.

In general, the components were selected to be standard parts wherever possible. RF electronics are highly sensitive to stray capacitances and inductances, therefore most dedicated RF components use surface mount⁴ (SMD) technology, sometimes even without pins. The passive components, like inductors, capacitors and resistors are in 0805⁵ sizing, which was deemed large enough to be still easy to solder by hand. All traces were impedance matched to 50Ω on standard 1.6 mm FR4 cards, milled with standard drill sizes to facilitate the use of affordable standard manufacturing processes. Lastly, SMA connectors were chosen for their small footprint and secure screw connection, as opposed to BNC connectors (large) and SMB connectors (less secure connection). Most parts were searched for using the parametric search functionality of the big distributors and filtered for only active, available and stocked parts — a rather large restriction in times of a global chip shortage.

3.1	THE CONSOLE	...	9	
3.2	THE POWER AMPLIFI	ER	13	
3.3	THE SWITCH	...	16	
3.4	THE PROBE	...	19	
3.5	THE LOW NOISE	AMPLIFIER	...	24
3.6	THE 32-CHANNEL	CURRENT SOURCE	...	26
3.7	THE MAGNET	...	29	
3.8	THE SOFTWARE	...	30	

1: Instruction for using the Red-Pitaya as an [LCR meter](#), [VNA](#), or spectrum analyser can be found in its documentation

2: ≈60CHF, <https://nanovna.com/>

3: ≈50CHF, <https://tinysa.org/>

4: as opposed to through-hole (SMT)

5: 0805 means 0.08 in x 0.05 in. PCB design is a mess of different unit systems, e.g. board sizes are often given in mm whereas trace width is often given in mil (thousandth of an in). Rarely 0805 is written as 2012M: 2.0 mm x 1.2 mm

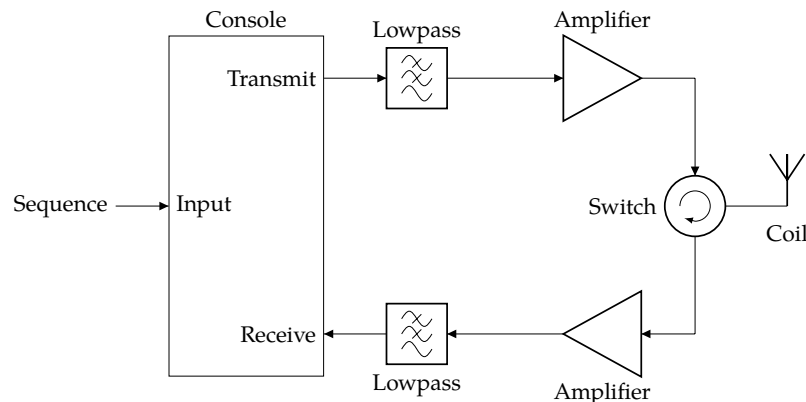


Figure 3.1: Block Diagram. The main components of the *magnETHical* NMR spectrometer, include the console, lowpass filters, analogue amplifiers, transmit-receive switch and transmit-receive coil.

Table 3.1: Comparison of different NMR spectrometer types. Prices are estimates based on previous purchases of the lab and experience in the price developments across vendors.

^awith/without shims

	Superconducting	Benchtop	<i>magnETHical</i>
Price [k CHF]	200–18 000	50–150	≈10
Frequency [MHz]	300–1200	40–125	25
Resolution [Hz]	≈0.2	0.2–1	≈2.5/50 ^a
Weight [kg]	600–15 000	25–150	≈5

In line with the goal of an accessible NMR spectrometer, the built spectrometer is very affordable. [Table 3.1](#) shows a comparison of it with a high-field spectrometer and other commercial benchtop spectrometers capable of measuring samples in a 5 mm NMR tube in terms of features.

[Table 3.2](#) shows a more detailed record of the prices of the individual components used and described in the following chapters. The vast majority of the money is spent on the magnet. Further development should seek better pricing here or start looking into home-made alternatives.

The section order follows the path of the signal, that is, clockwise around the schematic starting with the console.

	600 MHz ^a	mini-circuits	<i>magnETHical</i>
Power Amplifier	50 000	323.49	36.01
Switch	-	82.06	20.05
Probe	100 000	-	≈15.00
LNA	50 000	409.38	73.11
Shim Driver	-	-	257.08
Console	200 000	-	662.53
Magnet	1 000 000	-	≈9000.00
Sum			10 142.80

Table 3.2: Prices of the individual parts of the built spectrometer in comparison. Prices include VAT in CHF

^a estimated costs

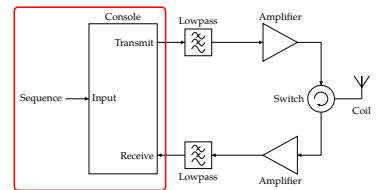
3.1 THE CONSOLE

The relatively low frequency of $f_0 = 25\text{ MHz}$ ⁶ as well as the low bandwidth of only about 10 ppm⁷ of the expected signal allows moving a lot of previously analogue tasks into the digital domain, greatly simplifying the hardware setup and making it more flexible. According to the Nyquist theorem, the minimum frequency that can be used to digitize an analogue signal without loss of information⁸ must be more than twice as large as the highest frequency component of interest in the signal. In our case, the analogue-to-digital conversion must happen with more than

$$f_{min} \geq 2f_0 = 50\text{ MHz}$$

if oversampling is to be used. The setup could also make use of the low bandwidth of the signal and use the aliasing effect of the analogue-to-digital conversion to its advantage using undersampling. Since this requires taking further care when sampling and filtering, and the expected frequencies are low enough to make oversampling feasible, oversampling is employed in this setup. This has the added advantage of higher flexibility since the sampling frequency can be easily adjusted downwards.

For digital processing, a **Field-Programmable Gate Array (FPGA)** is used, which can be thought of as a piece of programmable hardware. They have been successfully used in **NMR** spectrometers since 2007 to enable pulse generation and processing [11]. To ease development a ready-made **FPGA** board — the RedPitaya SDRlab 122-16 shown in Figure 3.2 — was chosen. With a sampling frequency of 122.88 MS/s it is well above the Nyquist limit. Combined with a resolution of 16 bit it is more than capable of capturing all relevant data from the



6: Given by the ^1H resonance frequency in the 0.6 T magnet

7: Equals 250 Hz at 25 MHz

8: That is, without aliasing issues

[11]: Takeda (2007), *A Highly Integrated FPGA-based Nuclear Magnetic Resonance Spectrometer*

9: For example Digikey, Mouser, Farnell, ...

10: [https://limemicro.com/
products/boards/limesdr/](https://limemicro.com/products/boards/limesdr/)

analogue signal. Due to the commercial nature, the board is easily procured directly from RedPitaya or any of the well-known distributors⁹. A possible open-source alternative in the future would be the LimeSDR¹⁰. With a sampling frequency of 61.44 MS/s, limited by the USB3 interface, and a resolution of 12 bit it is less powerful than the RedPitaya, but still fast enough for oversampling without loss of information. This board would cost less than half (≈ 280 CHF) of the RedPitaya board and would enable a completely open design of the spectrometer — in line with the accessibility goals of this work. Unfortunately, due to the young age of this project and the crowd-sourced nature, no board was available for purchase at the time of writing.

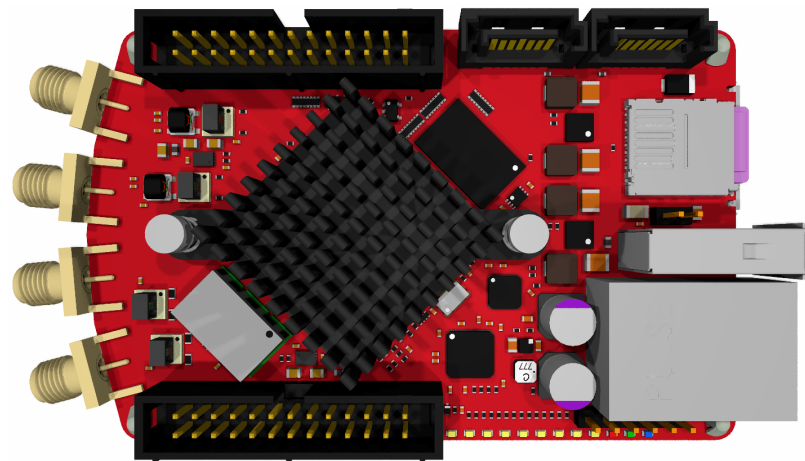


Figure 3.2: RedPiaya SDRLab 122-16. 3D rendering of the console in KiCAD. Can be thought of as an “RF Raspberry Pi”. It has a Dual Core ARM Cortex A9, 512 MB RAM, Gigabit Ethernet, 2x transmit, 2x receive, an ADC sample rate of 122.88 MS/s, 16 bit resolution, a bandwidth of 300 kHz to 550 MHz and a voltage range of $0.5 \text{ V}_{\text{pp}} / -2 \text{ dBm}$ (50Ω). The DAC has the same sample rate and voltage range, but a resolution of 14 bit and a bandwidth of 300 kHz to 60 MHz.

After sampling the signal is demodulated using a quadrature detection system by multiplying it with the signal of a complex numerically controlled local oscillator. The same principle is applied inversely on the sending side for modulation. The resulting complex demodulated signal is then passed through a [Cascaded Integrator-Comb \(CIC\)](#) filter for low-pass filtering and decimation to filter out high-frequency components of the signal and reduce the size of the data stream. The full data stream would incur a bandwidth of

$$16 \text{ bit} \cdot 122.88 \text{ MS/s} = 245.76 \text{ MB/s}$$

11: According to the official [LCR meter](#) documentation ([https://redpitaya.readthedocs.io/en/
latest/appsFeatures/applications/
streaming/appStreaming.html](https://redpitaya.readthedocs.io/en/latest/appsFeatures/applications/streaming/appStreaming.html))

12: [https://pavel-demin.github.io/
red-pitaya-notes/alpine/](https://pavel-demin.github.io/red-pitaya-notes/alpine/)

per channel. With potentially 2 transmit and 2 receive channels this results in a data rate of close to 1 GB/s, which is way higher than the theoretical limit of 116 MB/s of the Ethernet interface. Due to inefficiencies in the Linux kernel of the RedPitaya Image, the practical data rate limit for continuous streaming is a lot lower at about 20 MS/s¹¹. This has been improved in Pavel Demin’s kernel image, where speeds up to 80 MB/s have been measured¹². However, this only becomes relevant on

long acquisition times over several seconds and has not been thoroughly tested as it has not been relevant, yet.

All of these digital signal-processing tasks are performed by the [MaRCoS FPGA](#) firmware developed by Vlad Negnevitsky[12]. The system is designed for a low-field MRI system but could be easily adapted for NMR spectroscopy. The demodulated, filtered and decimated data from MaRCoS is then sent through its C server to the developed high-level Python interface. [Figure 3.3](#) shows an overview of the [MaRCoS](#) architecture. For more information on the Python programming interface see [Section 3.8](#).

[12]: Negnevitsky *et al.* (2023), *MaRCoS, an Open-Source Electronic Control System for Low-Field MRI*

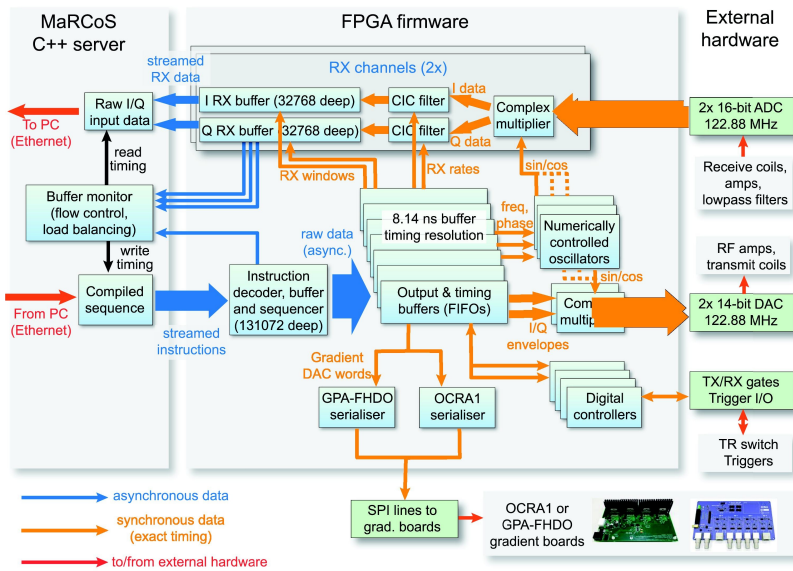


Figure 3.3: MaRCoS system architecture. “The server receives a sequence from the client PC via Ethernet and streams it to the FPGA firmware, where it is translated into time-synchronous hardware operations including RF and gradient outputs. The firmware receives data from the ADCs, demodulates and filters it, and saves it into RX buffers, from which it is read by the server and sent to the PC” ([12], Figure 3) Magnetic field gradients are not necessary for spectroscopy and thus not used.

The low-noise amplifiers before the receive inputs can output more than 20 dBm of power ([Section 3.5](#)). The maximum input the RP can handle before breaking is $1 \text{ V}_{\text{pp}}/4 \text{ dBm}$. Thus in case any RF signal gets leaked into the cascaded amplifier chain the inputs of the RP could be destroyed. To prevent this a pair of crossed shunt diodes is connected before the inputs.

The first obvious choice for this would be standard silicon diodes with a threshold voltage of about 0.7 V. The prototype with the standard BAV99 diodes would only clamp the signal safely to about 2 V_{pp} . The lower threshold voltage BYS10 Schottky diodes tried next behaved attenuated the signal by about 12 dB. The oscilloscope recording of a $100 \text{ mV}_{\text{pp}}$ sine wave of a function generator passed through the Schottky diodes is shown in [Figure 3.4](#).

A simulation confirmed later by measurement shows a phase shift between input and output occurs. This lead to the hypothesis that a high capacitance forming a filter with the 50Ω

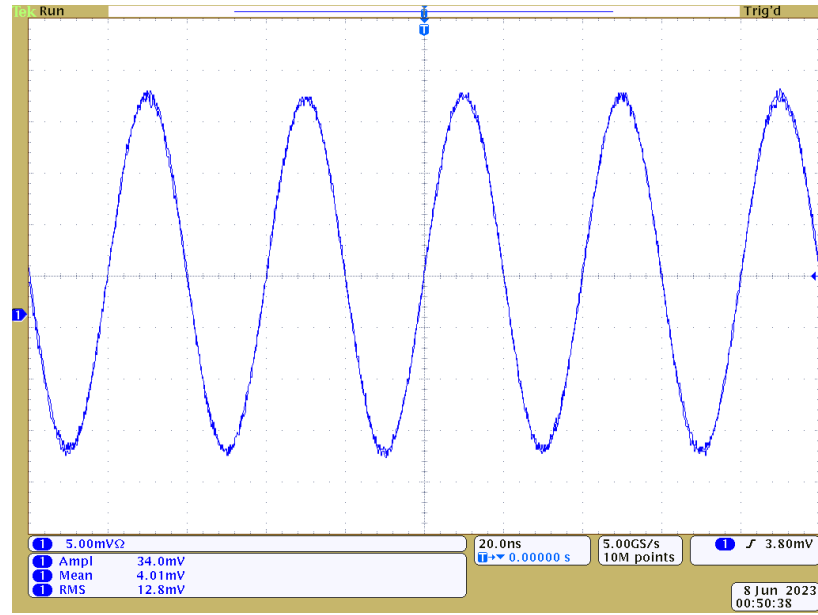


Figure 3.4: Receive input protection of crossed shunt BYS10 Schottky diodes attenuating the signal. The attenuation is unacceptably high. The input signal of $100\text{ mV}_{\text{pp}}$ is attenuated down to 24 mV_{pp} or by about 12 dB.

termination is responsible for the attenuation of the signal. Through a parameterized search the RB520SM-30 Schottky diode was found and then simulated to be suitable for the input protection. The measurement of the final version can be found in [Figure 3.5](#). While still attenuating the signal, only about 1.4 dB are lost while still clamping the maximum voltage to less than 1 V_{pp} .

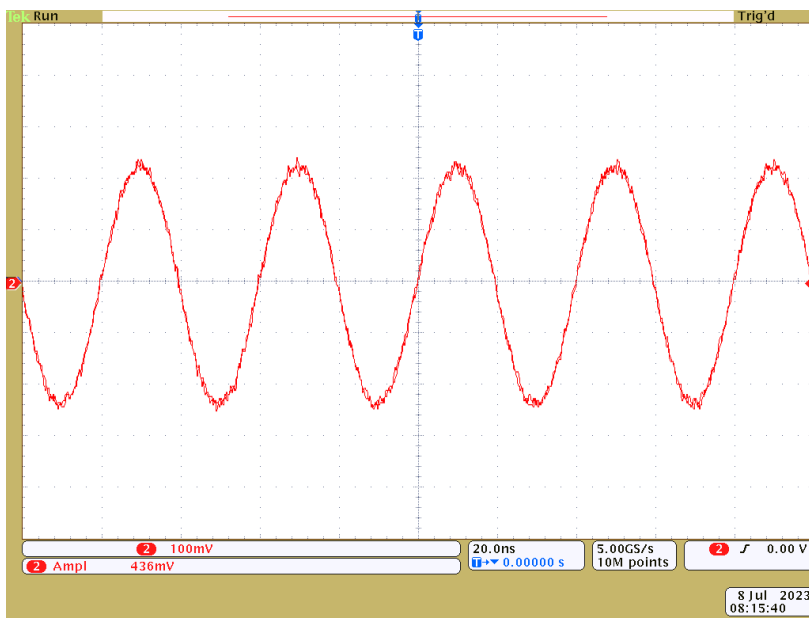


Figure 3.5: Working receive input protection of crossed shunt RB520SM-30 Schottky diodes. The Schottky diodes attenuate the 500 mV input signal to about 426 mV, equivalent to a power attenuation of 1.4 dB.

3.2 THE POWER AMPLIFIER

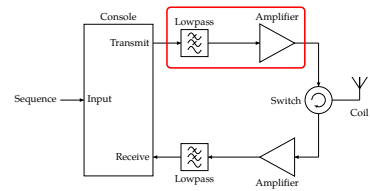
The power amplifier has to amplify the low-power digitally synthesised signal from the console. The console described in Section 3.1 above has a maximum output power of 0.5 V or -2 dBm into a 50Ω load.

The output power required to excite a volume of 1 cm^3 on a bandwidth of about 10 kHz or 20 ppm in a high field magnet (500 MHz (^1H))/ 11.7 T) is about 11 W [13]. The magnet in this work (see Section 3.7) has a field strength of 25 MHz (^1H)/ 0.6 T , therefore 20 ppm equals an excitation bandwidth of only 500 Hz . The sample volume is only $100\text{ }\mu\text{L} = 0.1\text{ cm}^3$ as well, reducing the required energy further.

Targeting a pulse length of $20\text{ }\mu\text{s}$ for a ^1H $\frac{\pi}{2}$ -pulse the RF pulse needs to generate a magnetic field of about

$$B = \frac{\alpha}{\gamma\tau} = \frac{\frac{\pi}{2}}{42.577\text{ MHz/T} \cdot 20\text{ }\mu\text{s}} = 1.845\text{ mT}$$

The magnet has a homogenous region of $100\text{ }\mu\text{L}$ for a 5 mm NMR tube, resulting in an NMR active length of about $l = 6\text{ mm}$. If we assume a simple solenoid of that length with about $n = 20$ turns, a Q factor of 100 (usually in the range of 10 to 1000 [14]) and a self-inductance of $L = \frac{\mu_0 n^2 A}{l} = 3\text{ }\mu\text{H}$ we can roughly estimate the required peak power P with the following formulas [14]



[13]: Louis-Joseph *et al.* (2019), *Designing and Building a Low-Cost Portable FT-NMR Spectrometer in 2019: A Modern Challenge*

[14]: Mispelter *et al.* (2015), *NMR Probeheads for Biophysical and Biomedical Experiments: Theoretical Principles and Practical Guidelines*

$$B = \frac{\mu_0 n I}{l} \quad (3.1)$$

$$P = R I^2 = R \frac{I^2}{2} \quad (3.2)$$

$$Q = \frac{L\omega}{R} \quad (3.3)$$

(3.4)

where B is the magnet field produced by the current I through a solenoid of length l with n windings and air core of permittivity μ_0 . P is the maximum power pushed into the solenoid by current I over resistance R and Q is the definition of the quality factor for a self-inductance L and resistance R . Putting it all together results in an estimated power level of

$$P = \frac{B^2 l^2 L \omega}{2 \mu_0^2 n^2 Q} \quad (3.5)$$

$$= \frac{(1.845 \text{ mT})^2 \cdot (6 \text{ mm})^2 \cdot 3 \mu\text{H} \cdot 2\pi \cdot 25 \text{ MHz}}{2 \cdot \mu_0^2 \cdot 20^2 \cdot 100} \quad (3.6)$$

$$= 457.12 \text{ mW} \quad (3.7)$$

The exact power required is difficult to calculate at best due to various losses of the materials, the sample, the surrounding materials and losses due to radiation. Previous works with low-field NMR spectrometers used power amplifiers with a maximum power output of 1 W [15] and 5 W [13]. Lower power RF amplifiers have the advantage of lower required voltages, lower noise, less cooling requirements and simpler integrated designs.

The most affordable option for the power amplification would be based on **RF** transistors. Unfortunately, this also necessitates an involved design process including not only biasing and feedback design, but also impedance matching and power supply circuits of a possible multi-stage power amplifier. This alone could be the topic of another thesis. Therefore, an **MMIC** approach has been chosen. Furthermore, availability in the 1 W range is large due to a large commercial market in this power range especially for CATV amplifiers. Therefore, a 1 W **MMIC** amplifier was chosen.

The **Monolithic Microwave Integrated Circuit (MMIC)** amplifier has biasing, possible feedback and stabilization requirements all integrated on a single substrate design. In an application only power, **DC** blocking in addition to adequate cooling have to be supplied, since this is a Class A amplifier design.

The final board can be found in [Figure 3.6](#), with its schematic in the appendix [Section A.1](#) and the part list in [Section B.1](#).

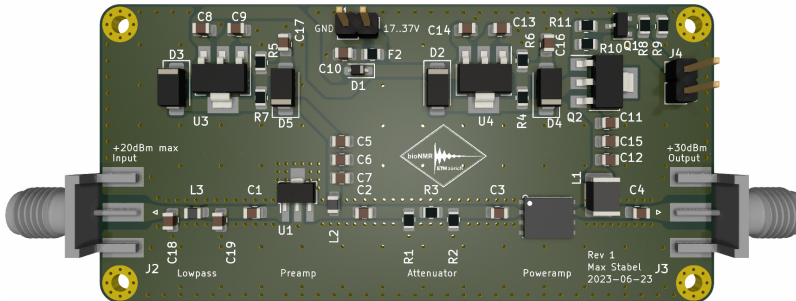


Figure 3.6: RF power amplifier. 3D rendering of the power amplifier PCB in KiCAD. The signal travels from left to right with the power supply circuitry above. It contains two MMIC amplifier stages, the AD5536 and the PHA-202+. A -6 dB attenuator was added in between and a passive low-pass filter in front ($f_c = 35\text{ MHz}$). $G \approx 32\text{ dB}$, $P_{1\text{dB}} \approx 30\text{ dBm}$

The signal from the RedPitaya travels left to right through a low pass, the pre-amplifier, an attenuator and the power amplifier. The parts at the top of the board are standard linear voltage regulators used for stabilizing the voltage from the external DC supply. The power amplifier chip itself can be switched off by cutting the voltage supply.

The low-pass input filter functions as a digital reconstruction filter, smoothing the digitally synthesised waveform by filtering out high-frequency components of the signal left over from the switching of the FPGA and the zero-order hold DAC chip. It is a passive Chebyshev low-pass LC ladder filter realized with three 0805-sized SMD components.

The power amplifier is a PHA-202+, chosen for its easy powering requirements, 50Ω matching and wide availability. However, it does not have enough gain (18.3 dB) to take the signal from -2 dBm all the way to 30 dBm . The missing 14 dB in amplification are provided by the preamp (20 dB) minus the following attenuator (6 dB).

The AD5536 pre-amplifier is a 50Ω matched, widely available 20 dB gain GaAs gain block from Analog Devices. It is in an easy-to-solder package and has a low enough frequency specification to work with 25 MHz. Alternatives with this gain and power are often difficult to solder due to the leadless design, unmatched (e.g. AFIC901N) 75Ω matched (e.g. MAAL-011139) and often cannot amplify such a slow signal (e.g. TAT7430B, starting at 50 MHz).

The 6 dB resistive attenuator in between the amplifiers is realized as a π -circuit similar to the low pass ladder filter. It is used to stabilize the adjacent amplifiers and will dampen any oscillations that might occur due to load or stray capacitances or inductances. If necessary the attenuation could be reduced to e.g. 3 dB to increase the maximum power output of the amplifier, however, since the $P_{1\text{dB}} = 29\text{ dBm}$ for the PHA-202+ it will not grow linearly. The potential distortions should be of little consequence for the transmission signal.

For blocking the DC bias current for the amplifiers simple 0805 100nF caps are used in series as a high pass filter. For a 50Ω system we can calculate the minimum value for the capacitors using the standard formula $X_C = \frac{1}{2\pi f C}$ and keeping in mind that the block is loaded on both sides thus $2 \cdot 50\Omega = 100\Omega$. For 25 MHz we thus get a minimum capacitance of

$$C = \frac{1}{2\pi f X} = \frac{1}{2\pi \cdot 25 \text{ MHz} \cdot 100 \Omega} = 63.7 \text{ pF}$$

The chosen 100 nF are significantly larger and simply chosen for convenience and availability. Their high-pass cut-off frequency is at

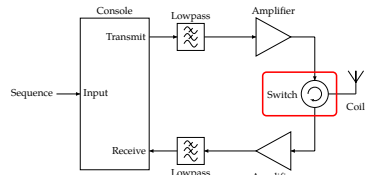
$$f = \frac{1}{2\pi X C} = \frac{1}{2\pi \cdot 100 \Omega \cdot 100 \text{ nF}} = 15.9 \text{ kHz}$$

13: Co805C104J5RACTU

14: <https://ksim3.kemet.com/capacitor-simulation>

For the chosen capacitors¹³ by KEMET this can be easily verified using the provided K-SIM simulator¹⁴, which confirms an insertion loss (S_{21}) of 0 dB and an input reflection (S_{11}) of -68 dB for 25 MHz.

3.3 THE SWITCH



[16]: Lowe *et al.* (1968), *A Fast Recovery Probe and Receiver for Pulsed Nuclear Magnetic Resonance Spectroscopy*

The switch has two main functions: 1. Protecting the receive path from the high power pulses when transmitting and 2. blocking the noise of the transmit power amplifier when receiving. The simplest approach for the user would be a passive switch, that does not need an active signal and simply forwards everything from the transmit port to the probe and everything from the probe to the receive port and nothing else. The possibly most popular design is the passive switch presented in [16] and pictured in Figure 3.7. It is based on easy-to-build, cheap and passive. On the downside, it has a narrow bandwidth, which is not a problem for our case, as the resonance frequency of the permanent magnet is fixed and varies only slightly.

The passive switch's working principle is based on the diode's characteristic to only start conducting above 0.7 V forward bias and RF wave propagation properties. When transmitting with high power, the wave amplitude is above 0.7 V. Since there is no DC bias the voltage also goes negative, hence the crossed diodes. They can therefore be thought of as shorts in this case so the pulse is sent from the transmit input port through point A in the centre to the probe connected at the top. Looking from point B towards ground it looks like a short-circuit as mentioned before. This short-circuit is then transformed by the $\frac{\lambda}{4}$ length cable so it looks like an open circuit when looking

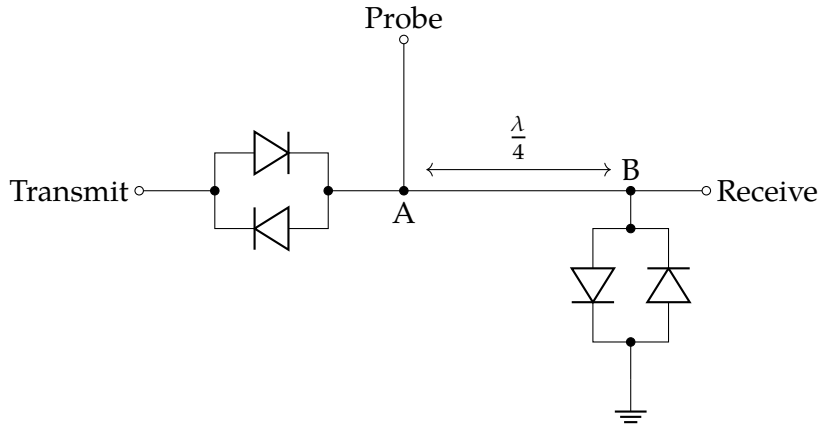


Figure 3.7: The passive switch. Based on Diodes and RF properties, the passive switch forwards the signal based on signal power. Due to the diode characteristics, the switch leaks up to 0.7 V without attenuation — including noise.

from point A towards point B. Therefore the only path the transmit pulse “sees” is towards the probe, because the receive port looks like an open circuit — there is nothing connected.

On the other hand, the received signal is very low in signal amplitude — low enough that the diodes do not start conducting. Therefore they function as an open circuit. The signal coming from the probe port travels therefore through point A to point B and into the receiver, ignoring the paths “disconnected” by the diodes.

This switch was built by the electronic workshop and can be found in [Figure 3.8](#). Instead of only one crossed diode pair four pairs were used. Since the wavelength of a $f = 25\text{ MHz}$ wave is about $\lambda = 12\text{ m}$, a “lumped element $\frac{\lambda}{4}$ -impedance transformer” was used which electrically simply looks like a 3 m cable. The circuit consists of an inductor in series and two shunt capacitors to its sides. To increase the attenuation of the signal the impedance transformer and diode subcircuit have been repeated three times in the realized circuit in [Figure 3.8](#).

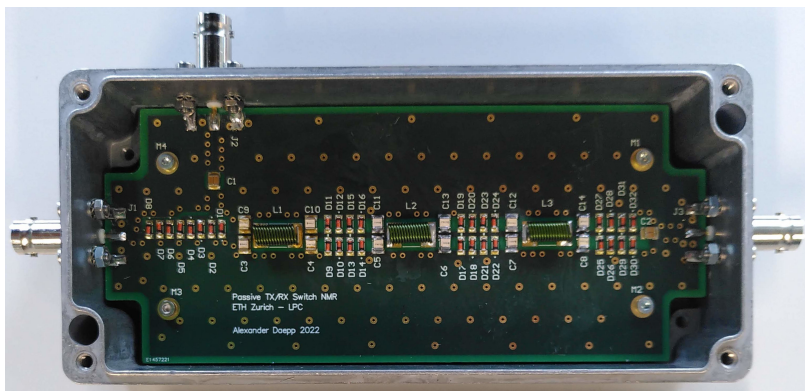


Figure 3.8: Passive RF T/R switch The power amplifier output would be connected on the left, the probe at the top and the low noise amplifier on the right.

Unfortunately, due to the diode characteristics, the switch leaked at least 7 dBm of power which would be amplified by the low noise amplifiers to levels that could damage other electronics downstream. Additionally, during receive the power amplifier would generate more noise than anticipated and the diodes would conduct lower voltages than calculated, therefore adding noise to the received signal that was orders of magnitude larger than the actual signal. For these reasons, active switch designs were explored.

The active design of this kind of switch is called **Single Pole, Double Throw (SPDT)** switch. A simple variant would be replacing the crossed diodes with biased PIN-diodes functioning effectively as **RF** switches. This kind of **SPDT** switch is very fast and conceptually simple. Unfortunately, they typically also suffer from worse isolation at lower frequencies and have a higher power consumption due to the biasing compared to **FET** switches. Biasing itself comes with its own challenges of mixing **AC** and **DC** usually using chokes and capacitors similar to the amplifier case. Lastly, many PIN diodes do not work at these low frequencies ($< 100 \text{ MHz}$) as the intrinsic region does not store enough charge for the negative half wave of the sinusoid.

Since the maximum power requirements are relatively low (see [Section 3.2](#)), integrated **FET** switches become a viable solution. These work by simply connecting the individual branches using **FET** transistors. Though slightly slower and less capable for higher power applications they provide very good isolation at these “low” frequencies in the MHz range. They are commercially widely available for use in wireless infrastructure due to their broadband handling capabilities. Many variants exist that are already matched to 50Ω and are absorptive in the off state. This helps with shortening the duration of the coil ringing and proves a safeguard for the power amplifier in case of misuse as most power amplifiers can be damaged when the output is open or unconnected like in a PIN-diode-based switch.

The Qorvo QPC6324 was therefore selected with a still acceptable insertion loss of 0.9 dB and a high isolation of over 60 dB, a $P_{1\text{dB}}$ of 37 dBm, 50Ω matched, absorptive ports and 3.6 V logic compatibility it is a good match for the circuit and easily controllable by the **General-Purpose Input/Output (GPIO)** pins of the RedPitaya. No external circuitry or **DC** blocking capacitors are needed, only a linear power supply to stabilize the input voltage and capacitances to limit the rise speed of the control lines were added to the **PCB** design in [Figure 3.9](#).

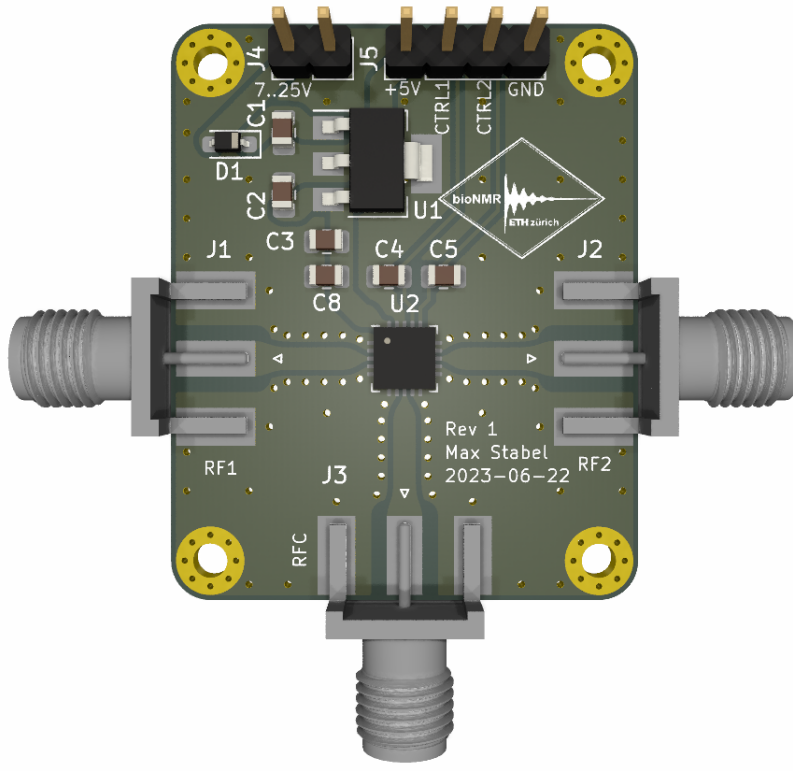


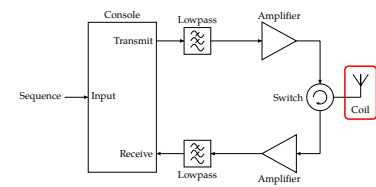
Figure 3.9: RFT/R switch 3D rendering of the switch PCB in KiCAD. The transmit and receive amplifiers are connected on the left and right, the probe at the bottom connector. The central part is a Qorvo QPC6324 Single Pole, Double Throw (SPDT) switch. Above it is a linear power supply and connection pins for active switching and power supply.

3.4 THE PROBE

To create the required B_1 field to perturbate the population of spin states in the sample an **RF** field needs to be generated¹⁵. There are many possible designs for this conversion from the transmission line, the simplest being a solenoid coil used here. Myriads of parameters can be optimized in the probe including its type, length, diameter, number of windings, and consequently self-inductance and Q-factor as well. However, the solenoid is probably one of the best designs in terms of sensitivity for NMR, even though the inductance increases rapidly with the dimensions. It is best used for small samples and/or low fields [14] — which is our case.

In addition the probe holder should position the sample correctly in the central homogeneous region of the magnet which is a 6 mm diameter sphere. To this end a custom 3D printed probe holder was created with the solenoid coil mounted including the tuning and matching circuit.

The manufacturer of the magnet made a probe to guarantee the specifications of the magnet. This holder can be seen in [Figure 3.10](#). Unfortunately, the design files for the probe holder were not made available and the probe is significantly smaller than



¹⁵: while an **RF** wave is generated as well, the far field is not used in the experiments and considered part of the loss.

[14]: Mispelter *et al.* (2015), *NMR Probeheads for Biophysical and Biomedical Experiments: Theoretical Principles and Practical Guidelines*

the space available in the magnet (50 mm x 55 mm x 9.5 mm), therefore correct positioning proved to be a challenge.



Figure 3.10: Manufacturer's probe holder and RF coil with tuning and matching capacitors
The body was 3D printed and the circuit cut by hand.

The solenoid coil consists of ≈ 0.2 mm insulated copper wire wrapped around a clear plastic tube in 18 turns on a length of 6 mm with a diameter of 7.5 mm resulting in a theoretical self inductance of

$$L = \frac{\mu_0 N^2 A}{l} = \frac{\mu_0 \cdot 18^2 \cdot \pi \cdot \frac{7.5 \text{ mm}}{2}^2}{6 \text{ mm}} = 3.00 \mu\text{H}$$

for a long air-filled coil. The self inductance of the coil inside the circuit (that is, with tuning and matching capacitors attached) was measured to be $2.3 \mu\text{H}$ at 1 kHz with a PM6303 RCL meter.

The tuning and matching of the probe was performed outside the magnet with the resulting curve in [Figure 3.11](#). The tuning and matching were very sensitive to the surroundings and should be redone inside the magnet when used for spectroscopic measurements.

In an attempt to overcome the shortcomings of the manufacturers coil a larger version of it that fills the available space inside the magnet was created. This parameterized 3D model designed using openSCAD was then exported to a standard 3D model format, sliced and printed. The first print was done on a Prusa MK3S MMU2S with 0.3mm PLA on the "DRAFT" setting in roughly 30 min. Due to small gaps at the connection joints of different parts it was printed again with a smaller print diameter of 0.2mm with the "QUALITY" setting which did not show any holes in 1.25 h and can be found in [Figure 3.12](#). The full dimensions are 70 mm x 83.35 mm x 10 mm, positioning the coil exactly in its center of the magnet.

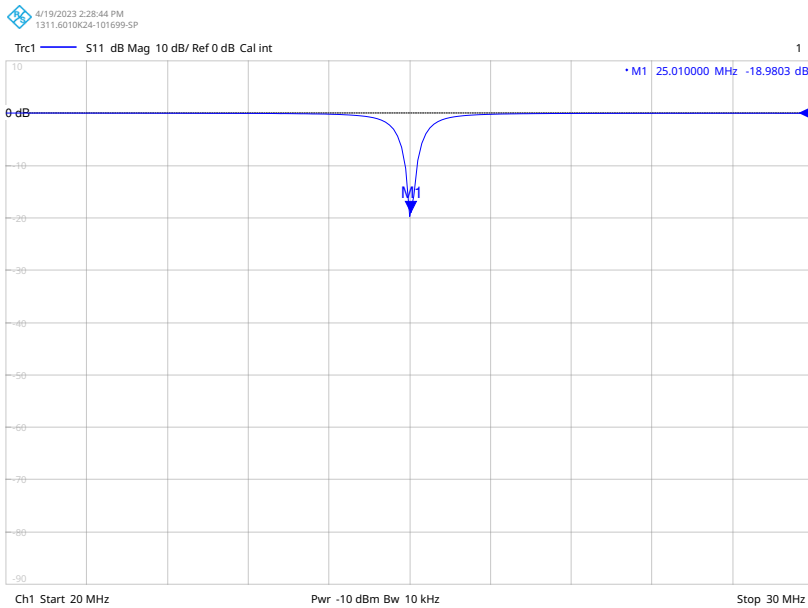


Figure 3.11: The S_{11} coefficient of the manufacturer probe On an x-scale from 20 to 30 MHz and a logarithmic y-scale in dB. Measured with a Rhode & Schwarz ZNB 4 VNA.

The coil was designed similarly to the manufacturer's probe as well. 0.2 mm diameter insulated copper wire was wrapped 18 times around a 7.5 mm glass tube on a length of 4 mm. This results in a theoretical inductance for a long air-filled coil of 4.5 μ H. To reach a resonant frequency of 25 MHz a tuning capacitance of about 9 pF is thus needed in theory in an LC circuit. When measured with an HP4284 LCR-meter while resting on a styrofoam box an inductance of 2.74 μ H and a resistance of 0.627 Ω was measured at 1 MHz. The difference can be attributed to stray capacitances of the connection wires, between the individual windings and the surroundings. The coil is also not long compared to the diameter — a different model would be more accurate.

To estimate the coil behaviour closer to resonance frequency a resonant circuit was formed by connecting a 10 pF capacitance to both ends and then measured using a pickup coil connected to a Rhode & Schwarz ZNB4 VNA. The resonant frequency was estimated to be 29.6 MHz using the well known LC resonance formula

$$f_{\text{res}} = \frac{1}{2\pi\sqrt{LC}}$$

the inductance was calculated to be

$$L = \frac{1}{4\pi^2 f_{\text{res}}^2 C} = \frac{1}{4\pi^2 \cdot (29.6 \text{ MHz})^2 \cdot 10 \mu\text{F}} = 2.89 \mu\text{H}$$

which is relatively close to the measured 2.74 μ H at 1 MHz.

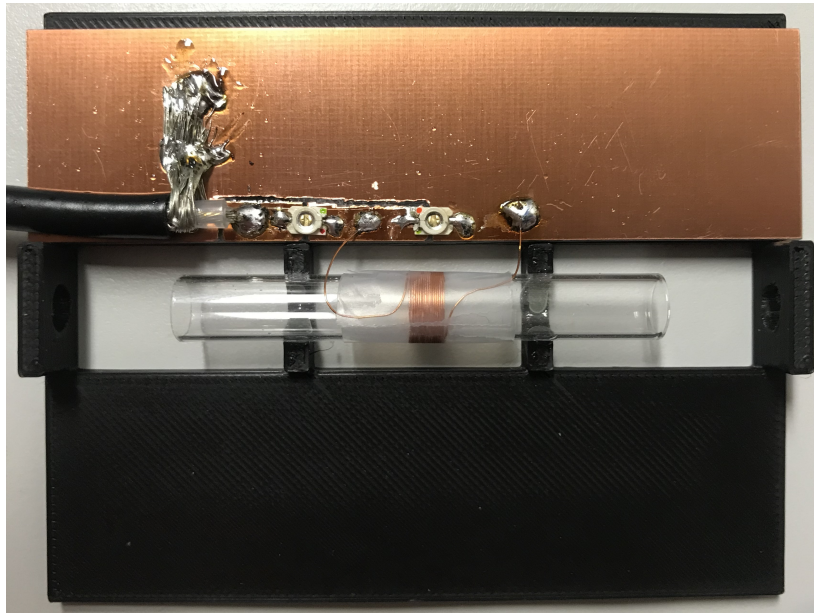


Figure 3.12: Probe holder and RF coil with tuning and matching capacitors The capacitors are tunable from 4.5 to 20 pF of make JZ200HV. The coil has a diameter of $d = 7.5$ mm, wire diameter $D = 0.2$ mm and $n = 18$ turns on a length of $l = 4$ mm. It has a measured inductance of $L_{1\text{MHz}} = 2.7 \mu\text{H}$ and a resistance of $R_{1\text{MHz}} = 0.63 \Omega$. The body was 3D printed and the circuit cut by hand.

16: JZ200HV

With the new inductance value, a capacitance of ≈ 14 pF is needed for resonance at 25 MHz. To allow for tuning and matching of the circuit two variable capacitors with a range of 4.5 to 20 pF was therefore chosen¹⁶. It is a high-voltage, paramagnetic model. Figure 3.12 shows the complete probe. The completed probe was then tuned and matched outside the magnet with the results depicted in Figure 3.13.

Despite the seemingly better tuning and matching of the signal of the home-built coil, the manufacturer's probe gave better spectra, i.e. more Lorentzian line shapes and a stronger signal. Qualitatively, the probe is less sensitive to stray capacitances and is better behaved inside the magnet, though this has not been quantified.

A lot more work can be done. The presented probe is utterly simple and functional, but by no means optimized. Different designs, parameters and configurations are to be explored. This includes saddle coils and variable pitch coils but also approaches like distributed capacitances between the windings of the solenoid coil. For more consistency, the winding patterns could be 3D printed as well.

Another important aspect is the shielding of the probe which would provide more defined stray capacitances and reduce induced noise from the environment. Since the magnetic field is relatively homogenous even outside the small specified volume, a second coil with a fixed known sample could be included in the probe holder for locking purposes, simplifying the processing. Lastly, the ability to tune and match the coil

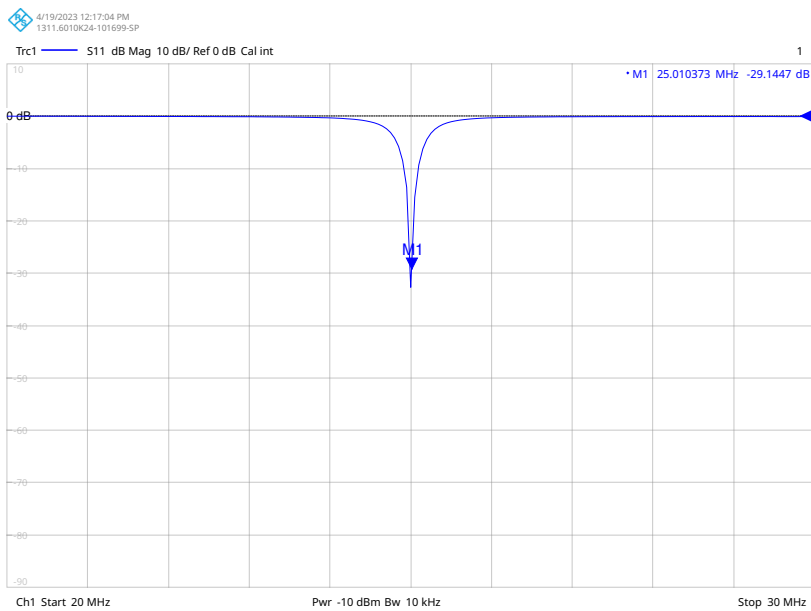
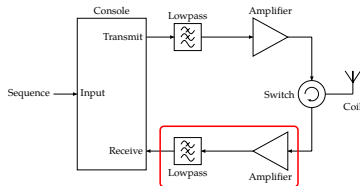


Figure 3.13: The S_{11} coefficient of the home-built probe On an x-scale from 20 to 30 MHz and a logarithmic y-scale in dB. Measured with a Rhode & Schwarz ZNB 4 VNA.

from the outside of the magnet would help greatly in usability.

3.5 THE LOW NOISE AMPLIFIER

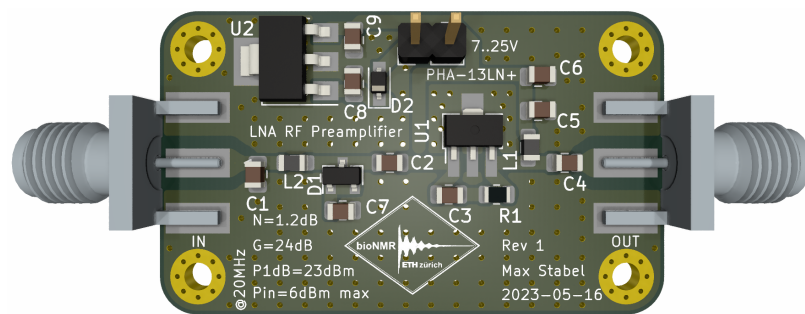


On the receive path, the first thing to do is amplify the weak resonance signal. To this end, an amplifier is needed to boost the signal from the μW level up to the measurement range of the **ADC** of about 0.625 mW without compromising the signal. To this end an amplification of more than 30 dB is needed, which generally implies a two or three-stage amplifier design. In principle, the first amplifier dominates the chain, as the noise introduced by it will be amplified by any subsequent amplifier in the chain. Despite this — for simplicity — the same low noise amplifier is used in all stages.

The low noise amplifier design follows largely the same principles as the power amplifier design. In [Figure 3.14](#) the signal travels from left to right first through a 1.8 GHz low-pass filter as recommended by the **LNA** manufacturer of the low noise amplifier in the datasheet to remove out of band frequencies that might cause distortions. Next is a set of crossed silicon diodes (BAV99) decoupled with a ceramic capacitor to prevent **DC** current flow. They prevent any surges or leaked pulse from damaging the amplifier that follows and clamp the voltage to about 5 dBm/1.2 V_{pp}. It then reaches the PHA-13LN+ amplifier which has a noise figure of $N = 1 \text{ dB}$ at 20 MHz. After the last amplifier a simple passive low pass filter (SCLF-27+) with a cut-off frequency of 27 MHz is added. It is added after the last amplifier to reduce its influence on the signal and because the saturation of the amplifiers due to out-of-band noise has not been an issue¹⁷. The full schematic of a single amplifier stage can be found in the appendix [Section A.3](#) alongside the list of parts in [Section B.3](#).

¹⁷: The out-of-band reflections of the filter have not posed any issue for the amplifiers either, but they were not specifically tested

Figure 3.14: The low noise amplifier 3D rendering of the low noise amplifier PCB in **KiCAD**. The signal travels from left to right through a low-pass filter with 1.8 GHz cut-off frequency, a 5 dBm clamping diode and the PHA-13LN+ low noise amplifier ($G = 24 \text{ dB}$, $N = 1 \text{ dB}$, $P_{1\text{dB}} = 23 \text{ dBm}$ @20 MHz). The power is supplied by the onboard linear regulator at the top



The design is inspired by the low noise **RF** pre-amplifier by the **RF Lab** of the **MR-PIG Group** at the **Martinos Center for Biomedical Imaging**¹⁸. It largely follows the recommended layout of the manufacturer with the addition of protection diodes and an included linear power supply. Furthermore,

¹⁸: https://rflab.martinos.org/index.php?title=Low-noise_RF_Preamplifier

care was taken to make the board easily reproducible using hand-solderable parts on a standard FR4 core **PCB**.

After assembly, the amplification performance of the amplifier was evaluated using a nanoVNA in [Figure 3.15](#). A single stage amplifies the signal by 23.21 dB — which is very close to the expected 23.62 dB at 30 MHz. The input return loss is slightly lower with 14.47 dB than the expected 16.04 at 30 MHz. The noise figure was measured to be 1.1 dB which is close to the specified 1.03 dB in the datasheet.

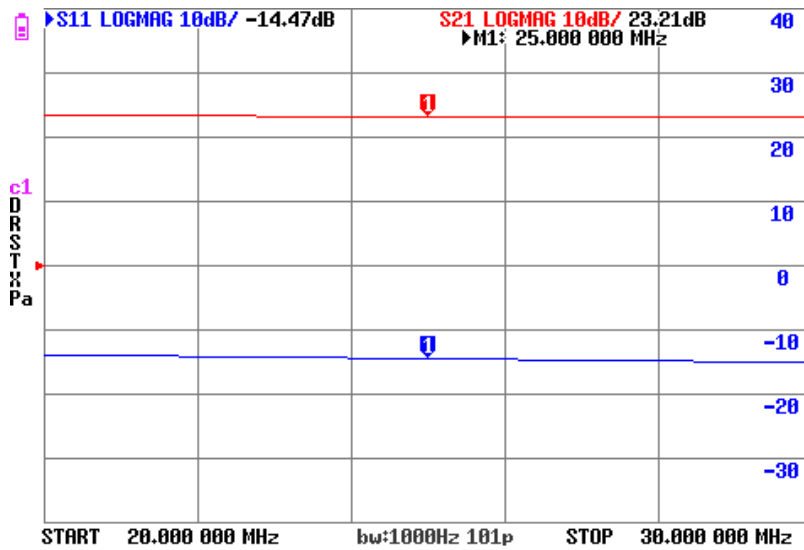


Figure 3.15: VNA S_{11} and S_{21} measurement. An S_{11} of -14.47 dB and a S_{21} of 23.21 dB was measured at 25 MHz using a nanoVNA-H4.

Upon concatenating the three amplifiers, spurious oscillations were noticed. Depending on load conditions, even a single amplifier would start oscillating. First, simple stray capacitances were tested as a possible source of the oscillations. For this different capacitances in the pF range were added between various components and various components and ground with no effect on the oscillations.

Having noticed that the stability factor (K-factor) is lowest and very close to one for the manufacturer evaluation board ($K = 1.01$) in the target frequency range, the feedback path was shortened and the 0805-sized capacitor and resistor (R_1 and C_3) were replaced with corresponding 0402-sized variants of otherwise the same specifications. This completely eliminated the oscillations in a single amplifier as well as the three-stage amplifier chain. To attenuate possible other oscillations, 3 dB attenuators were placed between the individual stages. The layout was fixed accordingly, but no new **PCB** with the fix included have been ordered.

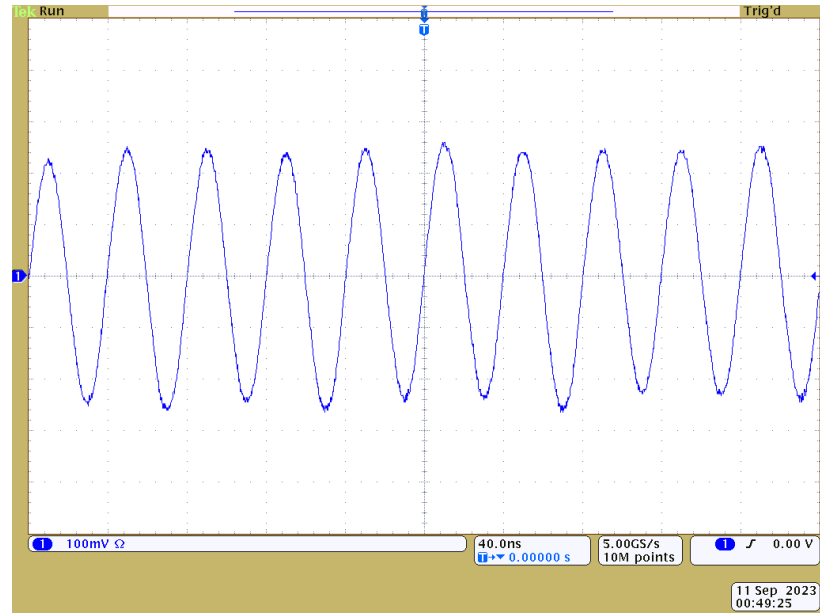


Figure 3.16: Amplifier concatenation test. Oscilloscope measurement of a function generator signal of $10\text{mV}_{\text{pp}} / -36\text{dBm}$ attenuated by $30\text{dB} (= -66\text{dBm})$ that was amplified by three low noise amplifiers built here separated by two 3dB attenuators and a low pass filter ($S_{21} < 0.3\text{dB}$) at the end. Expected total amplification is thus $G \approx 63.3\text{dB}$. Measured -2dBm equivalent to the full console input range, giving an amplification of 64dB .

3.6 THE 32-CHANNEL CURRENT SOURCE

The magnet was supplied with the active electronic shimming system already installed. They have a special design shown in [Figure 3.17](#) consisting of straight wires running across the pole faces — making good use of the limited space available between the two dipole magnets. The shim system consists of two PCBs with 16 different shims each that are together capable of generating the first through fourth order magnetic fields¹⁹ by supplying 32 individual currents. The resistance of each shim is about 0.2Ω .

19: with the exception of the fourth order $XY(X^2 - Y^2)$ field

To drive the shims, a 32-channel constant current source capable of driving $\pm 0.5\text{A}$ with a voltage range of $\pm 2.5\text{V}$ is needed. To this end multiple options were considered. Commercially available 32-channel digitally controllable current sources were deemed to expensive. Dedicated current control chips exist (e.g. MAX32010), though most only for single rail operation (e.g. HV9961, TLD1211SJ). Additionally they often don't have enough current drive capabilities, requiring an output stage which then again is often limited to single rail operation. Dual-channel operation needs at least twice the number of parts and additional balancing circuitry. The last option considered were LED driver ICs (e.g. NCR320PAS, LT3092) which are often only capable of single rail operation as well²⁰.

20: Which in hindsight makes sense, considering they drive diodes

[9]: Tietze et al. (2019), *Halbleiter-Schaltungstechnik*

The simplest solution for the problem as described in fundamental electronics textbooks (for example [9], page 771, chapter 11.3.1, implemented in [Figure 3.18](#) on the right) is using a non-inverting amplifier with the feedback path resistor

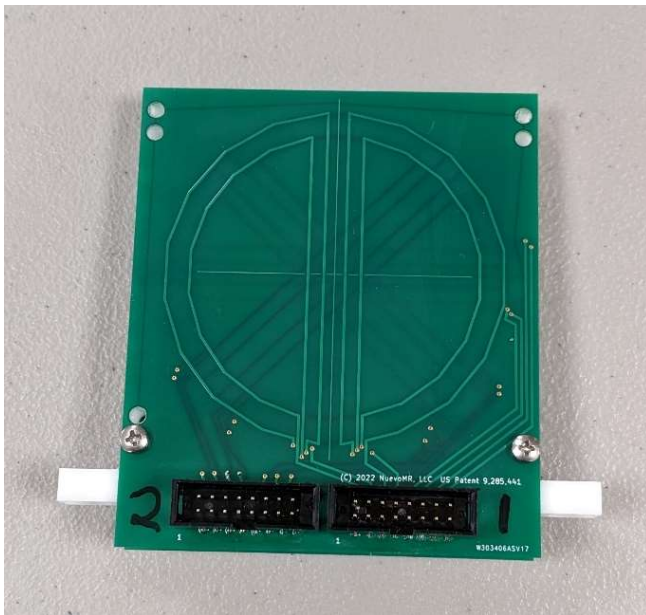


Figure 3.17: Active electronic shim system. The shown system was pre-installed inside the dipole magnet. The bottom side is shown, the top side is the equivalent. Current is supplied through the connectors at the bottom, each vertical pair connected to one shim.

exchanged for the load. This setup was used in the prototype built here, despite the disadvantage of the lack of specialised protection circuitry. Using a dual rail OpAmp capable of handling the high currents makes the circuitry quite easy.

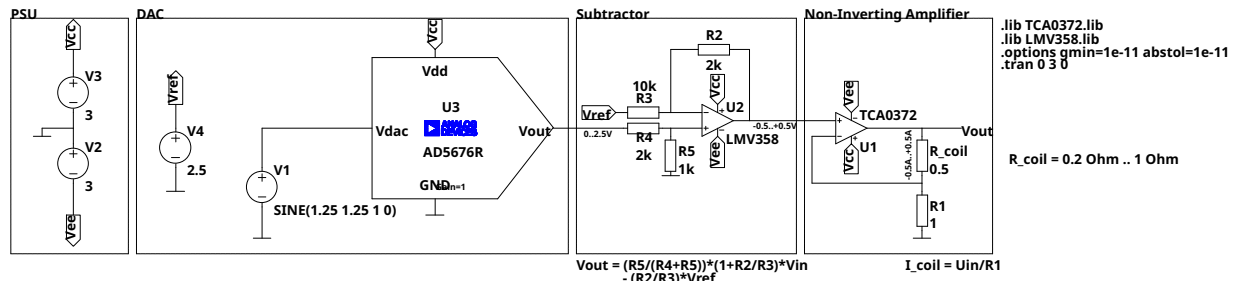


Figure 3.18: Simulation schematic of one channel of the current source in LTSpice. The output voltage of the AD5676R is in practice set through SPI by the console. It is important to not set the supply voltage too high, because excess voltage will drop over the OpAmp generating heat.

Figure 3.18 shows the LTSpice simulation of one of the 32 channels of the current source. The AD5676R Digital-to-analog converter (DAC) outputs a voltage between 0 to 2.5 V. The following subtractor circuit based on a LMV358 industry standard dual rail-to-rail output operational amplifier moves and scales this output to a voltage of -0.5 to 0.5 V before it is fed into the high power TCA0372 operational amplifier in a non-inverting amplifier configuration setting a constant current over R_{coil} . Figure 3.19 shows the output of the simulation of this circuit.

The AD5676R was chosen for its internal reference that further simplifies the circuit, its 16-bit accuracy and 8-channel output. It can be daisy-chained and thus controlled via a single SPI bus.

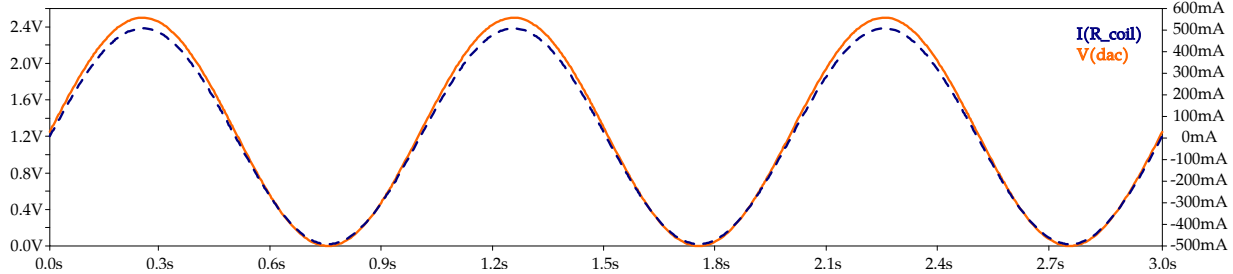


Figure 3.19: Simulation result of one current source channel. The dashed blue line is the resulting output current set by the output voltage of the [DAC](#) shown in solid orange. The curves deviate slightly, but this can be later corrected in software. Schematic of the simulation can be found in [Figure 3.18](#). Simulated using LTSpice.

A future prototype could have an integrated microcontroller to enable for example a [USB](#) interface.

Since the high power output [OpAmp](#) will operate in linear mode, excess voltage will drop over it and generate heat. Thus the voltage level should be chosen as low as necessary. To manage the excessive heat, VIAs were added below the operational amplifier on the board to help distribute the heat across the whole [PCB](#). Additionally, the bottom solder mask has been removed enabling good thermal connection to a heatsink attached to the bottom of the board.

21: the lid, screw and gasket have been hidden

[Figure 3.20](#) shows the final board inside the Hammond 1590Z150²¹ aluminium enclosure which doubles as a heat sink. The [SPI](#) interface on the right, the positive and negative power connectors on the left and the 32 output channels for the shims in the center. They are in assembly to be connected to the four connectors visible at the bottom of the picture in the sidewall of the enclosure.

Figure 3.20: 32-channel programmable current source. 3D rendering of the current source [PCB](#) in [KiCAD](#). The [SPI](#) interface is on the right, the power connectors on the left and the 32 output channels on the top and bottom of the [PCB](#). It consists of 4 8-channel [ADCs](#) (AD5676R) setting a voltage that is converted to a constant current by two [OpAmps](#): LMV358 for signal scaling and shifting and TCA0372 for the constant current source.



Each AD5676R [DAC](#) has 8 channels, each [OpAmp](#) package has two units inside, giving 4×2 channel per [DAC](#) that are replicated $4 \times$ across the [PCB](#).

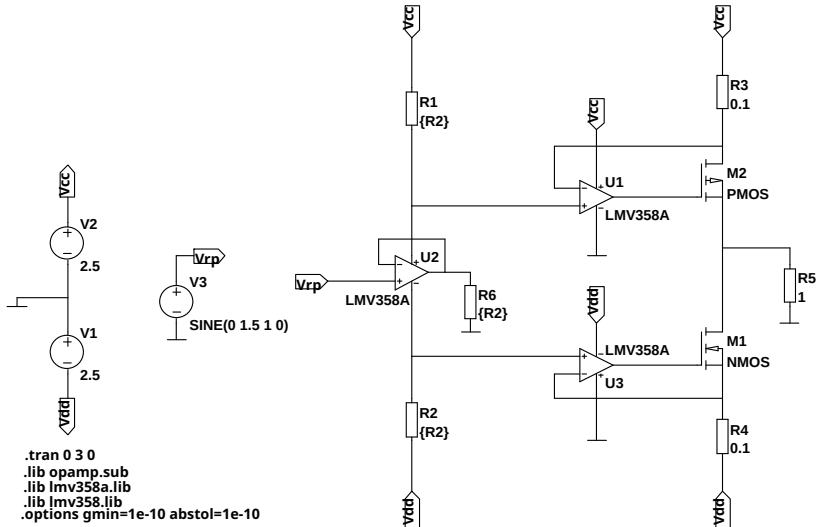


Figure 3.21: Alternative current source channel schematic. This push-pull circuit has higher current drive capabilities through the use of FET output stages. The zero point is compensated by the third OpAmp reducing quiescent currents compared to a resistor divider. Simulated in LTSpice, taken from [9] (page 778, chapter 11.3.3.1)

Unfortunately, there was not enough time to build and characterize the 32-channel current source for the shim drivers²². This exciting work has been left for the next person working on this project. If it works as intended with stable enough shimming results in the future different interface options and protection mechanisms could be added to make the driver more versatile. This includes over-voltage and over-current protection for inputs and outputs, temperature protection and fusing. If higher current drive capabilities are needed the slightly more complicated push pull configuration shown in Figure 3.21 could be used.

22: Which will become apparent in Chapter 5 later

3.7 THE MAGNET

The magnet was built by SABR Enterprises, LLC with a homogenous volume of $100 \mu\text{L}$ using a 5 mm NMR tube. It has a field strength of 0.6 T/25 MHz with a homogeneity of at least 0.1 ppm inside the homogenous volume with the magnetic ink shims and active electronic shimming performed by NuevoMR, LLC²³. A simple two-dipole setup is employed due to the ease of construction and shimming. The schematic can be found in the appendix Section A.5.

23: spherical harmonic fields of order 1-4 (except $XY(X^2 - Y^2)$)

A Halbach array — the so-called NMR Mandhala — was considered as well. While the achievable field strengths of 0.5 to 2 T [17] are sufficient, the initially achievable line width of 700 ppm [18] (without shims) magnets is not²⁴. This can be compensated by further passive and active shimming, at the expense of adding complexity to the design. The shimming of Mandhala magnets is still an ongoing research topic, see for

[17]: Blümich *et al.* (2014), *Compact NMR*

24: The chosen dipole magnet achieves a homogeneity of 4.7 ppm without active shims

[19]: Danieli *et al.* (2010), *Small Magnets for Portable NMR Spectrometers*

[20]: Parker *et al.* (2016), *Shimming Halbach Magnets Utilizing Genetic Algorithms to Profit from Material Imperfections*

[21]: Wang *et al.* (2022), *Design and Shimming Method of Low Length-to-Interdiameter Ratio Halbach Magnet*

example [19], [20] or [21] paper. This design is worth investigating further in the future promising low sub-kg weighta as well as price reductions — also considering the current price point for the dipole magnet of ≈ 9 kCHF.

For the material, temperature-compensated samarium cobalt (SmCo TC, EC 2:17-TC16) with a reversible temperature coefficient (RTC) of $-0.001\text{ \%}/\text{K}$ was chosen. The more common and cheaper Neodymium is more temperature sensitive with an RTC of around $-0.1\text{ \%}/\text{K}$. Due to the low field, multiple scans will likely be required for at least some NMR measurements, exasperating the undesirable effect of a field drift over longer periods.

3.8 THE SOFTWARE

The low-level **MA**gnetic Resonance **C**Onrol System (**MaRCoS**) software has been introduced in [Section 3.1](#). The **MaRCoS** client library sends “msgpack” formattted data from the PC to the C++ server running on the console, which handles sequence compilation and stream management with the **FPGA**. Around this client client library a simple interface for sending and receiving pulse sequences has been built.

Using “nmrglue” [22] it is possible to save the data in the popular NMRPipe [23] data format. This could easily be extended in the future to include for example the relatively new nmrML[24] open data standard or the older JCAMP-DX [25] format. The software adds simple processing and analysis shortcuts for 1D NMR spectra to facilitate easy and quick inspection of the data. This includes plotting, fourier transform, automatic phase correction, scale conversions, peak picking and single peak as well as spectra fitting.

The usage of the software is described further in [Chapter 4](#). Additional information can be found inside the repository including example scripts, demonstration notebooks, **CLI** documentation and an **API** reference.

[22]: Helmus *et al.* (2013), *Nmr-glue: An Open Source Python Package for the Analysis of Multidimensional NMR Data*

[23]: Delaglio *et al.* (1995), *NMR-Pipe: A Multidimensional Spectral Processing System Based on UNIX Pipes*

[24]: Schober *et al.* (2018), *nmrML: A Community Supported Open Data Standard for the Description, Storage, and Exchange of NMR Data*

[25]: McDonald *et al.* (1988), *JCAMP-DX: A Standard Form for Exchange of Infrared Spectra in Computer Readable Form*

THE COMPLETE SPECTROMETER

4

*Es wächst zusammen,
was zusammengehört.*

— Willy Brandt

The following sections look at the built spectrometer from a user's point of view. The first [Section 4.1](#) describes the assembly and operation of the spectrometer built above. The following sections set up the console ([Section 4.2](#)) and control software ([Section 4.3](#)). Lastly, [Section 4.4](#) discusses the how to measure a signal with a simple and approachable example.

4.1 SOFTWARE SETUP

The spectrometer was designed with ease of use and reconfigurability in mind. The individual parts are placed on separate boards, connected with standard [SMA](#) connectors. Broken parts can thus be easily exchanged. Old already existing parts can be used in conjunction with newly developed ones, facilitating the re-use of hardware and ensuring operation while a broken part is fixed or upgraded.

The software – while still incomplete – has the same goals as the hardware. It is written in [Python](#) with extensive documentation, comments throughout the code and accompanying guides to get started¹. Generally, the code tries to adhere to the ideas presented in “Uncle Bob’s” book *Clean Code* [26].

There are five main parts to the spectrometer as explained in [Chapter 3 \(The spectrometer\)](#):

THE CONSOLE (i.e. the RedPitaya) responsible for sending, receiving and processing the [RF](#) signals.

THE POWER AMPLIFIERS responsible for amplifying the signal generated by the console

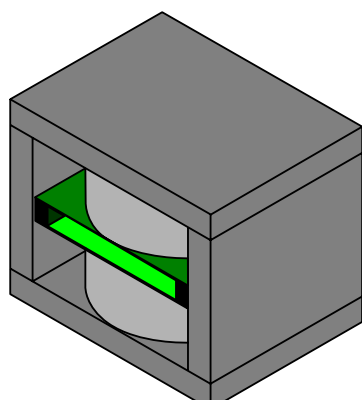
THE TRANSMIT-RECEIVE SWITCH responsible for switching between sending a signal into the probe from the transmit channel and receiving a signal back from the probe into the receive channel

THE PROBE consisting of the probe holder and the probe coil, responsible for emitting and receiving the [RF](#) signal

4.1	SOFTWARE SETUP	31
4.2	SETTING UP THE REDPITAYA	32
4.3	SETTING UP THE CONTROL SOFTWARE	33
4.4	PERFORMING A MEASUREMENT	34
4.5	EDITING THE CON- TROL SOFTWARE	36

¹: Take a look at the official `README.md` in the [official repository](#)

[26]: Martin (2008), *Clean Code: A Handbook of Agile Software Craftsmanship*



magnETHical

Figure 4.1: Logo of the *magnETH-*

THE **LOW-NOISE AMPLIFIERS** responsible for amplifying the weak signal received by the probe before feeding it to the console for processing

The short conceptual overview is reproduced in figure [Figure 4.2](#) for the reader's convenience. Each output needs to be connected to the input of the next device. The power connections are not shown in favour of clarity, but each part is labelled with the possible input voltages, in a range of 7 to 15 V. For a more detailed description of the individual parts and their connections see the *magnETHical* project page (compare [Figure 4.1](#)) or the descriptions above.

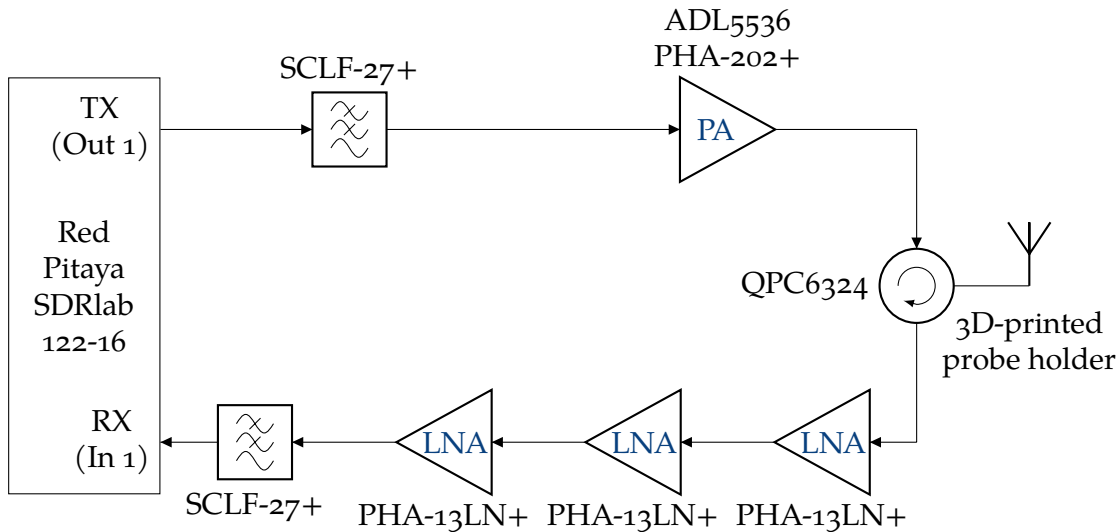


Figure 4.2: Component overview. The schematic contains all physical parts of the **NMR** spectrometer that need to be connected through **SMA** cables.

4.2 SETTING UP THE REDPITAYA

²: Again, see [Chapter 3](#)

Having ordered or built the parts², connected them using **SMA** cables and powered them through a lab power supply, the console needs to be configured. The configuration of the console is relatively simple as most of the complexity has been programmed into the **Python** control library. The user thus only needs to ensure that a working **Linux** distribution is running on the **RP** and that the **IP** address is known. The official distribution that is pre-installed on the micro SD card that ships with the **RP** is completely sufficient.

If the user needs to create a new microSD card, the [setup of the microSD card is described in the RP docs](#) and is summarized here for simplicity on a Linux based system.

1. Download the newest microSD card image

2. Insert the microSD card into your computer.
3. Determine its name using `lsblk` or `df -h`, e.g. `/dev/mmcblk0` or `/dev/sdc`.
4. Copy the image on the microSD card using
`dd bs=1M if=red_pitaya_image_file.img of=/dev/mmcblk0 status=progress`

5. Done!

The RP needs to be reachable through Ethernet from the computer running the control software. The easiest way is to connect them both to a **DHCP** server³ in the same network and lookup the IP address it got assigned by entering the name printed on it into a web browser. For a manual setup method for a direct connection in an isolated lab environment, see the `README.md` in the control software repository or the **Static IP configuration guide in the RedPitaya documentation**⁴.

The control software needs to be able to remotely log in to the system through **Secure Shell (SSH)**. For this, the `sshd` server needs to be running, which is the case for almost any image you find – including the official RedPitaya image⁵.

It is highly recommended to set up a passwordless login scheme from the computer to the RP. Listing 1 presents the necessary commands for creating a keyfile and copying it to the RP on a Linux machine. When asked, accept the recommended settings for the keyfile – do not set a password for it! Enter your password when prompted to do so.

```
1 | $ ssh-keygen -t ed25519          # create a keyfile
2 | $ ssh-copy-id root@rp-xxxxxx.local # alternatively: root@192.168.1.100
```

3: An example for a **DHCP** server would be any router or WiFi access point that automatically provides you internet access.

4: For this document we assume the RedPitaya is reachable on the IP `192.168.1.100`

5: The default username is `root` and the default password is also `root`. Sometimes there is no password – in that case, just press “Enter” when asked for one. Remember nothing – not even stars – is displayed when typing the password

Listing 1: Generating SSH keyfiles for passwordless login. Accept default configurations when prompted.

4.3 SETTING UP THE CONTROL SOFTWARE

On the computer, you need `git` and `python3` to run the software. On Linux, they can usually be installed with one of the commands in Listing 2.

```
1 | $ dnf install python3 git      # (Fedora/RHEL/CentOS/...)
2 | $ apt install python3 git     # (Debian/Ubuntu/Mint/...)
3 | $ pacman -S python git       # (Arch/Manjaro/Artix/...)
```

Listing 2: Installing prerequisites

With the prerequisites installed, the user can now install the spectrometer control software `Python` package. However, it is generally recommended to use “virtual environments”⁶ that create a new environment with packages and executables separate from the system and other programs. This functionality is

6: For more details see [PEP 668](#) and [PEP 405](#)

already included in [Python](#). Listing 3 describes how to set up and activate a new “virtual environment” inside a `~/spectrometer` folder.

Listing 3: Set up of a “virtual environment” (often called “venv”) in [Python](#)

```

1 | $ cd ~
2 | $ mkdir spectrometer
3 | $ cd spectrometer
4 | $ python3 -m venv .venv
5 | $ source .venv/bin/activate      # Linux
6 | $ .venv/bin/activate.ps1        # Windows Powershell
7 | $ .venv/bin/activate.bat        # Windows Cmd

```

The user can now install the control software including all dependencies independently from the system they are working on using the commands in Listing 4. The second one might take a while to run.

Listing 4: Installation of the python library with automated dependency resolution using [pip](#). Assuming the user already installed and activated a virtual environment as described in Listing 3.

```

1 | $ git clone https://github.com/M4a1x/nmr-spectrometer.git
2 | $ python3 -m pip install ./nmr-spectrometer/software/spectrometer

```

The installation process automatically adds scripts for controlling the spectrometer to the command line seen in Listing 5. These can be used to manually flash the firmware, set up the spectrometer hardware, and start the sequence processing server.

Listing 5: Command line spectrometer control commands

```

1 | $ magnethical flash_fpga
2 | $ magnethical setup
3 | $ magnethical start
4 | $ magnethical stop
5 | $ magnethical is_running

```

4.4 PERFORMING A MEASUREMENT

With the package and all dependencies installed as described above, the system is ready to be used. The software and hardware support arbitrary pulse sequences with one transmit and one receive channel⁷. A simple example is described here, for a more in-depth explanation of all the different functions, please look at the [API](#) reference in the repository. More examples for measurements are available as well — in particular, all measurements described below in [Chapter 5](#) are located in the `scripts` folder inside the Python package as well as a full demo notebook⁸ inside the `docs` folder.

⁷: This could be expanded software side to 2 receive and 2 transmit channels

⁸: To be precise: a [Jupyter Notebook](#). It is a tool for integrating Python code with text blocks and inline outputs making data analysis and plotting more convenient.

```

1 # Import the necessary packages
2 from spectrometer import (
3     Server,
4     ConnectionSettings,
5     Spectrometer,
6     NMRSequence,
7     FID1D
8 )
9
10 # Connect the server platform (i.e. the RedPitaya)
11 server = Server("192.168.1.100")
12
13 # Flash the FPGA bitstream (or "low level server")
14 server.flash_fpga()
15
16 # Compile the server on the spectrometer (or "high level server")
17 server.setup()
18
19 # Start the server on the spectrometer
20 server.start()
21
22 # Setup the spectrometer connection
23 connection_settings = ConnectionSettings(ip_address="192.168.1.100")
24
25 # Create the spectrometer object
26 spectrometer = Spectrometer(
27     tx_freq=25_091_000, # Center transmission frequency
28     rx_freq=None, # Receive frequency
29     sample_rate=320_000, # samples/second
30     server_config=connection_settings,
31 )
32
33 # Connect to the spectrometer server
34 spectrometer.connect()
35
36 # Define and send the sequence
37 seq_simple = NMRSequence.simple(pulse_length_us=9, delay_us=25,
38                                record_length_us=20_000)
39 data = spectrometer.send_sequence(seq_simple, debug=True)
40
41 # Save
42 fid = FID1D(
43     data=data,
44     spectral_width=spectrometer.sample_rate,
45     carrier_freq=0.0,
46     observation_freq=spectrometer.rx_freq,
47     label="1H",
48     sample="Water",
49     pulse="single_90_degree_pulse,length=9us,delay=30us",
50     spectrometer="magnETHical v1.0",
51 )
52 fid.to_file("my_experiment.fid")
53
54 # Plot, e.g.
55 fig = fid.plot()
56
57 # Spectrum
58 spectrum = fid.spectrum() # zero-fill, FFT, zero-order phase correction
59 fig = spectrum.hz.plot()
60 fig = spectrum.ppm.plot()
61 fit_spectrum, fitpeaks = spectrum.hz.fit()
62 peaks = spectrum.hz.peaks()

```

Listing 6: Performing a measurement on a sample using the control software. The hardware is assumed to be set up, connected and powered up. The 5 mm NMR tube with the sample should be inside the probe holder that was inserted into the magnet and the connection between the RedPitaya and the Laptop running the control software was verified. The code sends a single pulse of 9 μ s, waits for 25 μ s, records the received signal and plots it in the time and frequency domains.

4.5 EDITING THE CONTROL SOFTWARE

9: unittests are individual tests of separate components as opposed to integration tests that verify the interplay and compatibility of several units

The source code of the control software can be easily obtained through git as done in line 2 of Listing 7. It uses hatch for package and dependency management, which needs to be installed globally. hatch then provides commands for running a demo Jupyter notebook, unittests⁹, compiling and reading the documentation. The demo does not work offline and needs a connection to the spectrometer. The documentation and unittests are standalone. See Listing 7 for examples on using the commands.

Listing 7: Using hatch to perform common tasks when editing the control software. The invoked commands can be found in the pyproject.toml file in the repository. Examples for using the library are available in the scripts and docs folders.

```

1 $ python -m pip install hatch # Install globally with no venv activated
2 $ git clone https://github.com/M4a1x/nmr-spectrometer.git
3 $ cd nmr-spectrometer
4 $ hatch run demo # Open the demo Jupyter notebook in a browser
5 $ hatch run docs # Compile and open the documentation and API reference
6 $ hatch run test # Run the unit tests
7 $ hatch shell     # Activate the virtual environment

```

5

EXPERIMENTAL RESULTS

*Assumption is the mother
of all fuckups.*

— Wethern's Law

5.1	MEASURING A WATER SIGNAL . . .	37
5.2	MEASURING A TOLUENE SIGNAL .	44

The following presents the measurement results of different pulse sequences sent with the spectrometer and analysed with the control software. The code used to obtain these exact measurements can be found in the repository inside the `scripts` folder, and the raw data inside the `data` folder.

5.1 MEASURING A WATER SIGNAL

Probably the simplest NMR pulse sequence consists of a single $\frac{\pi}{2}$ -excitation pulse as seen in Figure 5.1. Inserting a standard 5 mm NMR tube filled with water with the probe holder inside the magnet, an experiment can be performed using the commands described in Section 4.4. Before the experiment, the $\frac{\pi}{2}$ -pulse length has manually been determined to be 8 μs by varying the pulse length, finding the length of a π pulse and confirming that a pulse of half the duration gives a maximum signal. The coil rings less than 25 μs , confirmed by looking at the received signal through an oscilloscope. Figure 5.2 shows the real part of the received signal from a water probe after the coil ringing.

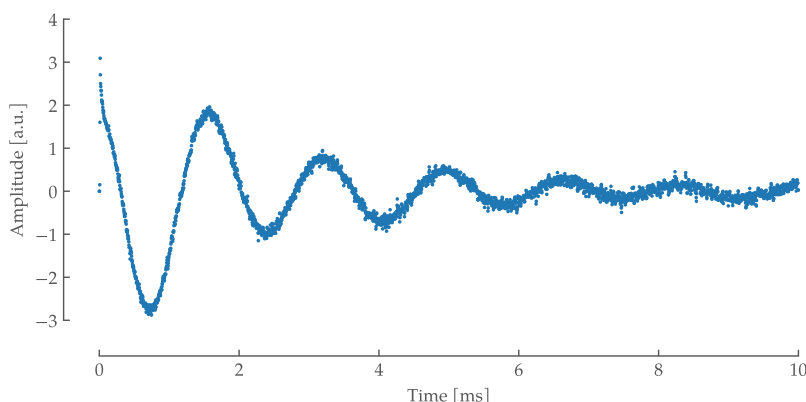


Figure 5.2 shows a nice exponentially decaying sine wave. There are some points at the beginning of the signal that clearly do not fit in this model. They can be explained through the

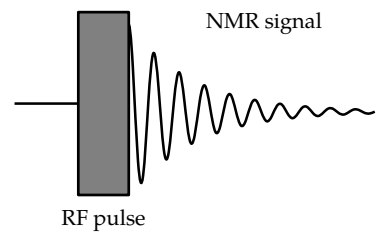


Figure 5.1: Simple pulse sequence The usual depiction of a simple pulse sequence. The “RF pulse” is a high frequency RF pulse close to the resonance frequency of the nuclei to be observed. After the pulse, a decaying cosine signal can be received on the same coil - the so-called Free Induction Decay (FID).

Figure 5.2: Free Induction Decay (FID) of water. The signal was recorded after a 8 μs impulse of a strength of 1 W and a delay of 25 μs , waiting for the coil to ring down. “Andrew’s probe” was used in this measurement with a transmit frequency of 25.09 MHz

impulse response of the discrete CIC filters and should ideally be discarded. Nevertheless, Figure 5.3 shows a least squares optimized fit of a decaying exponential sinusoid. Despite the outliers in the beginning this works quite well and confirms the first impression.

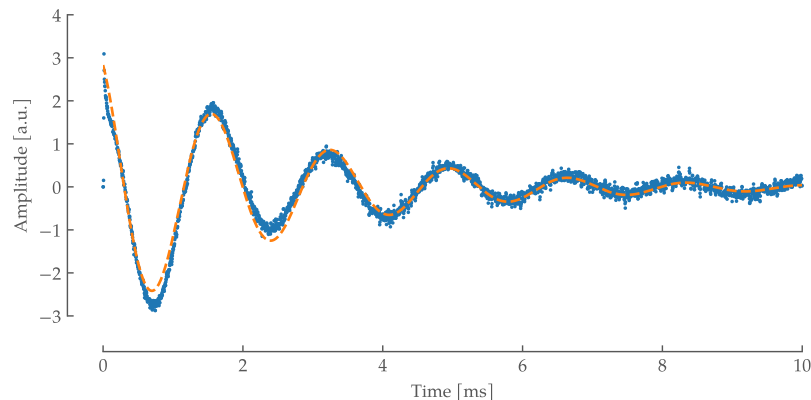


Figure 5.3: Free Induction Decay (FID) of water with a sine fit. The blue data is the same as in Figure 5.2. The orange dashed line is the result of a least squares fit of a decaying sine wave. It shows an exponential decay in amplitude with a T_2^* of 2.5 ms and a dominant frequency of about 590 Hz

The decay constant T_2^* of 2.5 ms is relatively short. In a properly shimmed high-field spectrometer it would be expected to be a few seconds — several orders of magnitude higher. The discrepancy can easily be explained by the lack of any active shimming. Therefore, a slightly different magnetic field acts on the individual water molecules, causing them to have slightly different resonance frequencies. As a result, they will de-phase quickly.

The Fourier spectrum in Figure 5.5 was obtained through zero-filling the data, a complex discrete Fourier transform and an automatic zero order phase shift. As expected we obtain a single peak stemming from the two magnetically identical ^1H in water, whose chemical structure is shown in Figure 5.4.

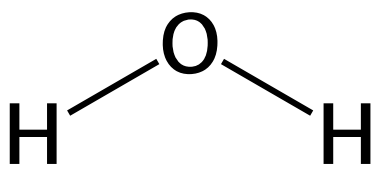


Figure 5.4: Structure of H_2O . Observe the two H atoms that should result in an identical NMR signal.

The shape seems almost Lorentzian, except for two deviations: (1) The (here small) broadening on the right side, which could be explained by the lack of active shimming and (2) the baseline distortion around the peak, which can be explained through the first erroneous points in the FID and the window effect of cutting off the signal in the beginning and end.¹ The shimming error could be a Z^2 shimming error, see [27] for examples of different kinds of shimming errors and their influences on the spectrum.

Performing a least-squares fit again the two deviations become even more apparent as seen in Figure 5.6. Even without shimming the linewidth is relatively narrow with a full width at half maximum of 118 Hz or about 4.7 ppm.

1: See for example the right side of Figure 2.1 in the concepts chapter. Remember, that figure shows the absolute amplitude, not the real part

[27]: Miner *et al.* (1997), *Shimming Ain't Magic - The Shimming of High Resolution NMR Magnets*

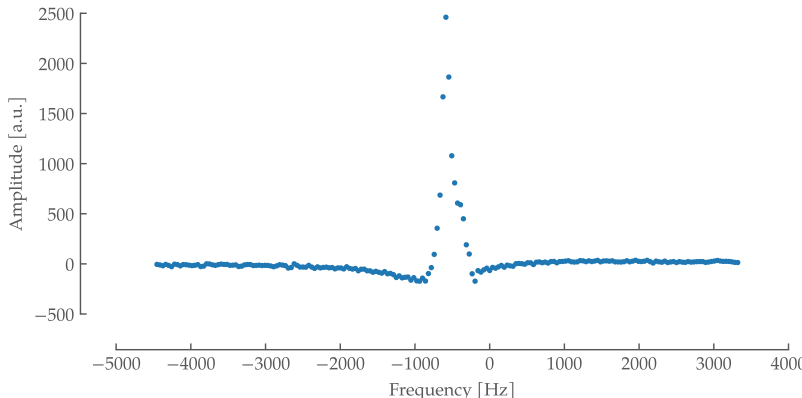


Figure 5.5: Fourier spectrum of Figure 5.2. It shows a Lorentz-shaped peak around roughly 600 Hz with a slight broadening on the right side and a distorted baseline. The data was obtained through an automatic zero fill, complex Fourier transformed and automatically zero order phase corrected with a shift of 37°.

The Fourier spectrum can be used to easily estimate the **Signal-to-Noise Ratio (SNR)** of the signal. With only one peak this is especially easy. The noise is estimated by calculating the standard deviation under the assumption that the expected value μ is 0, which works by modelling it as a sum of **Independent and Identically Distributed (IID)** random variables or more specifically **Gaussian White Noise (GWN)**².

The engineering definition of the **SNR** is the power P of the signal S divided by the power of the noise N :³

$$\text{SNR}_{\text{Engineer}} := \frac{P_{\text{signal}}}{P_{\text{noise}}} = \frac{E[S^2]}{E[N^2]}$$

The expected value is defined as

$$\mu_X := E[X]$$

The variance (also called the second central moment) is the square of the standard deviation, defined as⁴

$$\sigma_X^2 := E[(X - \mu_X)^2] = E[X^2] - E[X]^2 \stackrel{\mu_X=0}{=} E[X^2]$$

The variance of the signal itself is 0 as well⁵. Therefore we can simply write equivalently

$$\text{SNR}_{\text{Engineer}} = \frac{\mu_S^2}{\sigma_N^2}$$

In NMR spectroscopy the SNR is usually defined with the amplitudes as opposed to the power used in engineering. Taking the square root the above equation becomes

$$\text{SNR}_{\text{NMR}} = \frac{\mu_S}{\sigma_N}$$

2: Due to the central limit theorem for large n

3: S and N being random variables

4: The last equality being the reason the **Root Mean Square (RMS)** ($E[X^2]$) is often confused with the **Standard Deviation (STD)** $E[(X - \mu_X)^2]$. In experimental sciences μ is often assumed to be 0

5: In theory the signal without noise does not change across multiple experiments

6: The proof of which is left as an exercise to the reader

Using the above definition the noise was estimated by calculating the σ_N from 1 to 2 kHz and using the peak amplitude as the mean μ_S for the signal under the aforementioned assumptions. With an amplitude of 2505 and a noise of 7.83 this results in an SNR_{NMR} of 320 for the water spectrum.

For a constant area under the curve (i.e. constant signal strength) the SNR_{NMR} for a lower linewidth due to shimming can be estimated. In this case, the amplitude and the half width at half maximum are inversely proportional⁶. Assuming a resolution (i.e. full width at half maximum) of 2.5 Hz/0.1 ppm can be achieved as stated by the magnet specification and given an amplitude of 2505 on a linewidth of 118 Hz/4.72 ppm an SNR_{NMR} of

$$\text{SNR}_{\text{NMR,shimmed}} = \text{SNR}_{\text{NMR}} \cdot \frac{\text{FWHM}_{\text{measured}}}{\text{FWHM}_{\text{expected}}} = 320 \cdot \frac{118}{2.5} = 15\,066$$

is achievable.

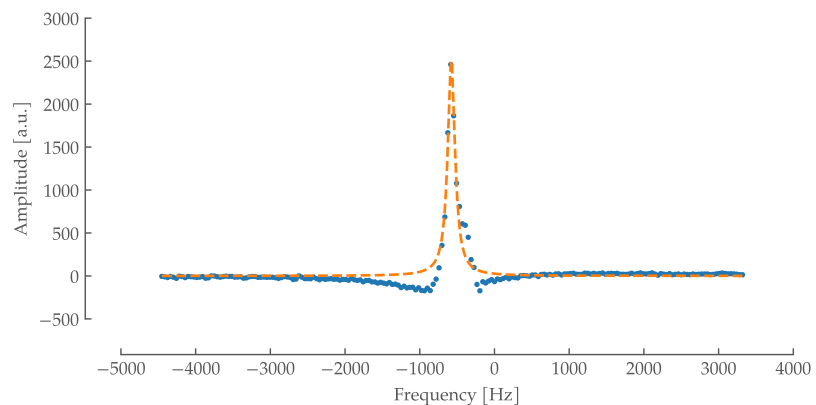


Figure 5.6: Fourier spectrum of Figure 5.2 with lorentzian fit. The Lorentzian curve was fit using a least-squares minimization approach. It is centred around -576 Hz with a full width at half maximum of 118 Hz resulting in a T_2^* of 2.7 ms.

To systematically find the pulse lengths required for various flip angles — most importantly the $\frac{\pi}{2}$ -pulse length used above — the above experiment can simply be executed with varying pulse lengths. The resulting “signal strength” is measured by integrating the area under the peak in the Fourier spectrum. To keep the phase information, an automatic phase correction is performed only once on a strong signal received after a pulse of roughly $\frac{\pi}{2}$. The same zero-order phase correction is then applied to the Fourier transforms of all pulse lengths. Plotting this signal strength measure over the length of the pulse that caused it in μs results in Figure 5.7.

7: the macroscopic sum of all magnetic dipole moments of the nuclei

8: Referring to maxima *and* minima

It clearly shows a decaying sine wave. The magnet causes the magnetization⁷ to align along the z-axis. We are measuring in the xy-plane. Therefore, the signal is strongest⁸ when applying a pulse of a duration that rotates the spins by $\frac{\pi}{2}$ along the x- or y-axis or its $\frac{\pi}{2} + n\pi$ multiples in the rotating reference

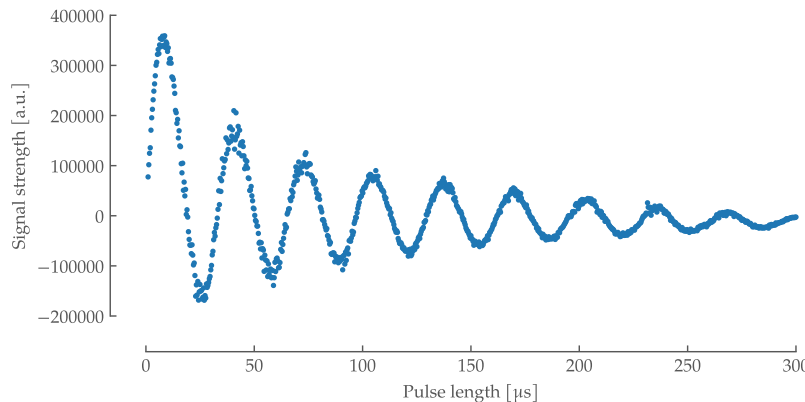


Figure 5.7: Rabi nutation of the water signal. Each data point was generated by performing an FID experiment as described in Figure 5.2 and integrating over the resulting peak (see Figure 5.5) to obtain a measure of signal strength. The zero-order phase correction applied to all points was identical.

frame (see e.g. [28] for a more in-depth explanation of the concept). The zero crossings are consequently at $n\pi$ multiples for integer $n = 1, 2, \dots$. With 3 rotations taking roughly $100 \mu s$ we can estimate a $\frac{\pi}{2}$ -pulse length of $100 \mu s \div (4 \cdot 3) = 8.3 \mu s$.

[28]: Keeler (2010), *Understanding NMR Spectroscopy*

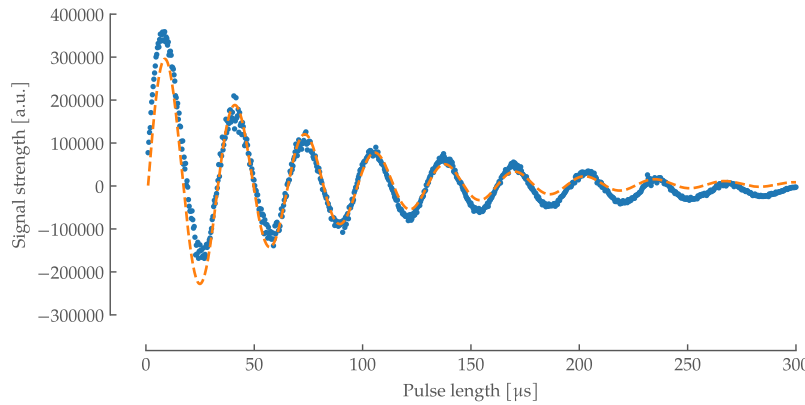


Figure 5.8: Rabi nutation of the water signal with decaying sinus fit. The data was fit using a least-squares approach to fit a decaying sinusoidal function. The fit has a period of $32 \mu s$, giving the length of a $\frac{\pi}{2}$ -pulse of $8 \mu s$.

Figure 5.8 shows the result of a least-squares fit of a decaying sinusoid to the data. This is a simple way to determine the frequency of the oscillation. The fit directly returns a period of $32 \mu s$, thus a $\frac{\pi}{2}$ -pulse length of $8 \mu s$ — confirming the estimation above.

The decay of the signal can be explained again with the dephasing of the spins. Due to the inhomogeneous magnetic fields the different nuclei experience, they resonate at different frequencies. A T_2^* of only 2.5 ms already has a significant impact in this timeframe and is not negligible anymore compared to the pulse length.

Without electronic shims the FID decay T_2^* is quite fast with a $1/e$ time of 2.5 ms. To measure the transversal relaxation time T_2 independently of the homogeneity of the magnetic field — thus dropping the * — a so-called spin echo experiment can be used. Figure 5.9 on the side shows the spin echo pulse sequence.

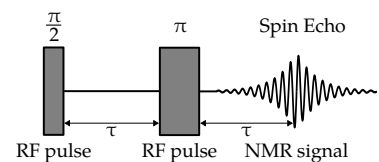


Figure 5.9: Spin echo sequence. A possible depiction of the spin echo sequence. A pulse of a duration that causes a $\frac{\pi}{2}$ rotation of the spins and a pulse twice as long (i.e. length π) are applied with a delay of duration τ in between. A spin echo is then observed with its peak after a delay of τ after the second pulse.

The idea of the spin echo sequence is that after the $\frac{\pi}{2}$ -pulse another π -pulse is sent after a delay of τ , effectively inverting all the spins. In the presence of an inhomogeneous field with the spins rotating at slightly different frequencies in the rotating reference frame, this π -pulse inverts consequently the direction of their de-phasing, causing them to align again when all spins returned to the starting point.

"This is analogous to an egalitarian foot race for the kindergarten class, the race that makes everyone in the class a winner. Suppose that you made the following rules. Each kid would run in a straight line as fast as he or she could and when the teacher blows the whistle, every child would turn around and run back to the finish line at the same time. The 180° pulse is like that whistle. The spins in the larger field get out of phase by $+\Delta\theta$ in a time τ . After the 180° pulse, they continue to precess faster than M but at 2τ they return to the in-phase condition. The slower precessing spins do just the opposite, but again rephase after a time 2τ " [29].

[29]: Suzuki *et al.* (2011), *Lecture Note on Senior Laboratory Spin Echo Method in Pulsed Nuclear Magnetic Resonance (NMR)*

Figure 5.10 shows the recorded signal after the π -pulse. A weak FID is visible directly after the π -pulse. This can be explained by inaccurate pulse lengths. If the duration is slightly off both pulses will add their errors together since they rotate the spins around the same axis. There are more sophisticated sequences that compensate for this, but this is outside the scope of this text.

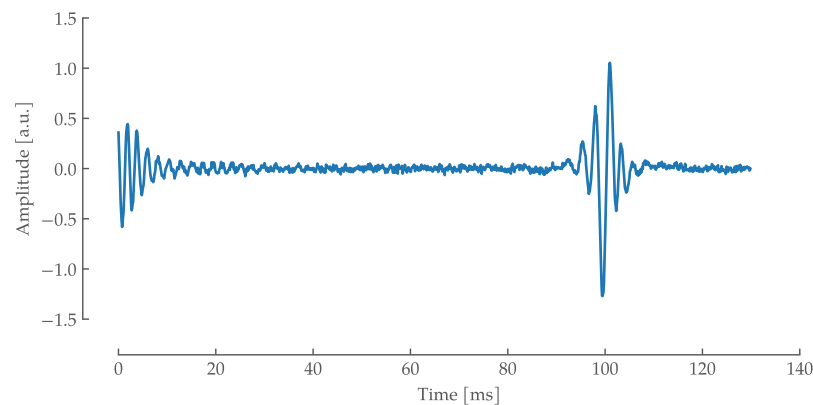


Figure 5.10: Spin Echo. Measurement of the received signal after the last pulse of a classic spin echo sequence (see Figure 5.9). The $\frac{\pi}{2}$ of $9 \mu\text{s}$ was sent with a power of 1 W. The delay between pulses τ was 100 ms. Data was recorded for 130 ms after the last pulse.

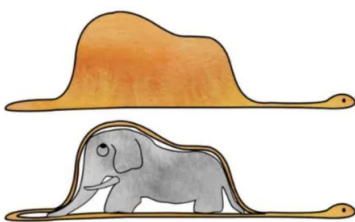


Figure 5.11: Le Petit Prince. "My drawing was not a picture of a hat. It was a picture of a boa constrictor digesting an elephant." — Antoine de Saint-Exupéry

The weak FID quickly decays until only noise is left. Then, the spin echo reappears much later centred exactly at 100 ms (the delay τ). Notice the different timescale compared to the simple FID experiment: A clear echo is still visible after 100 ms as opposed to ≈ 15 ms before. This confirms the previous hypothesis that the short relaxation time of the FID is due to the inhomogeneities of the unshimmed magnet. Much like looking inside that hat in The Little Prince (Figure 5.11), this

lets us catch a glimpse of the undisturbed nature of the atomic spins.

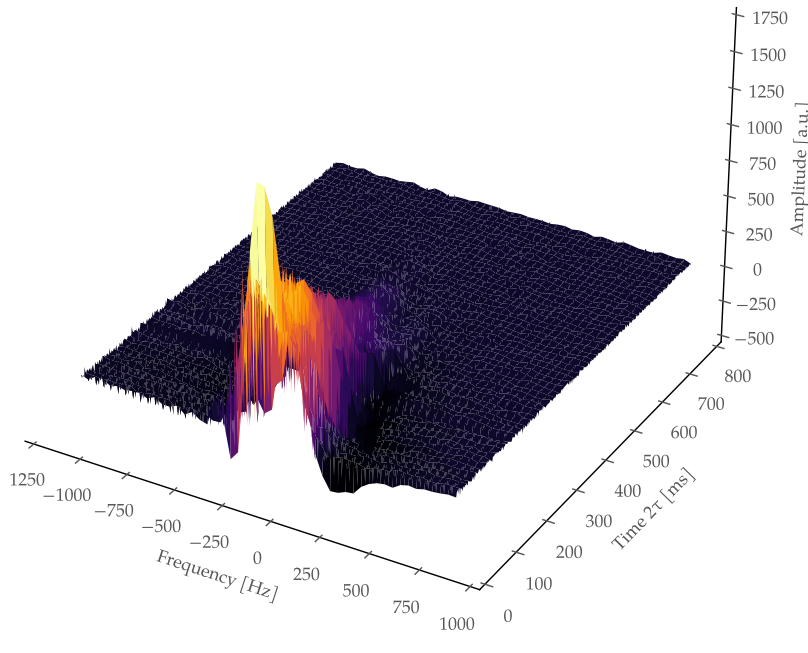


Figure 5.12: Fourier Transform of decaying spin echoes over delay length τ . The phase-corrected Fourier transforms are plotted in three dimensions over the delay τ in between the pulses. The decay of the signal strength with increasing delay is clearly visible.

The right half of the spin echo (starting at 2τ) can be interpreted as an FID again and Fourier transformed. Additionally varying the delay results in [Figure 5.12](#). It shows clearly the decaying amplitude of the central peak in the spectrum for increasing delay τ . Similar processing to the Rabi nutation experiment above, integrating over the spectra as a measure for “signal strength”, but plotting over 2τ results in the 2D plot in [Figure 5.13](#). The plot visualizes the decay of the signal with increasing τ even better.

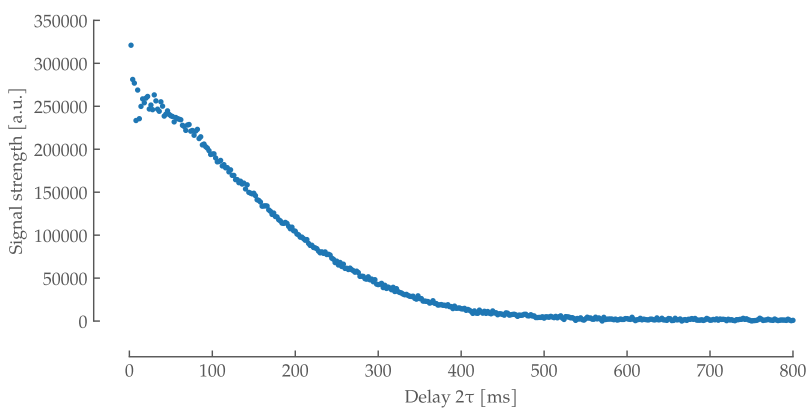


Figure 5.13: T_2 decay of water. Each data point is obtained by integrating the peak of the phase-corrected Fourier spectrum of a spin echo experiment as seen in [Figure 5.12](#). One can vaguely discern the expected exponential decay.

Performing a least-squares optimized fit of an exponential function results in the orange curve in [Figure 5.14](#). The T_2 fit of 190 ms is as expected orders of magnitude higher than the T_2^* of 2.5 ms measured above.

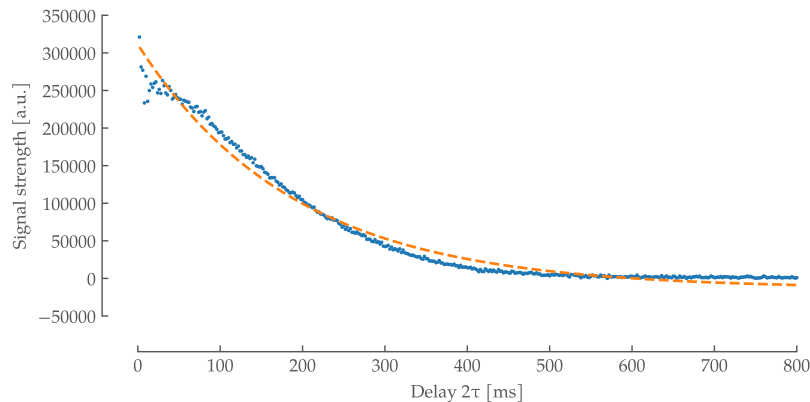


Figure 5.14: T_2 decay of water with an exponentially decaying function fitted. The data points are the same as in Figure 5.13. The least-squares fit has a T_2 decay time of 190 ms.

5.2 MEASURING A TOLUENE SIGNAL

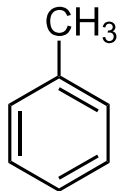


Figure 5.15: Chemical structure of Toluene. Notice the two main components: The CH_3 Methyl group on one side and the Phenyl ring on the other. The hydrogen atoms in both have very distinct NMR resonance frequencies and differ by about 5 ppm.

The following paragraph analyses the signal of an NMR test tube filled with pure Toluene. Looking at the chemical structure in Figure 5.15 we expect two groups of signals. One from the CH_3 Methyl group and one from the Benzene ring. The different spins of the H nuclei in the benzene ring could be differentiated if the resolution of the spectrometer was high enough — even with shimming this would be challenging with a low-field magnet of 25 MHz.

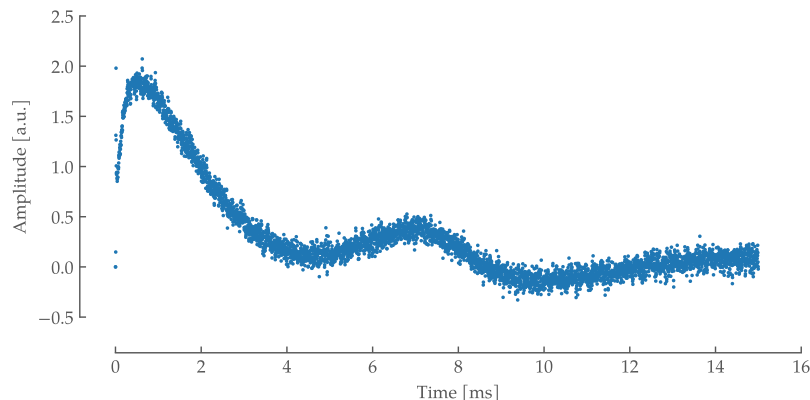
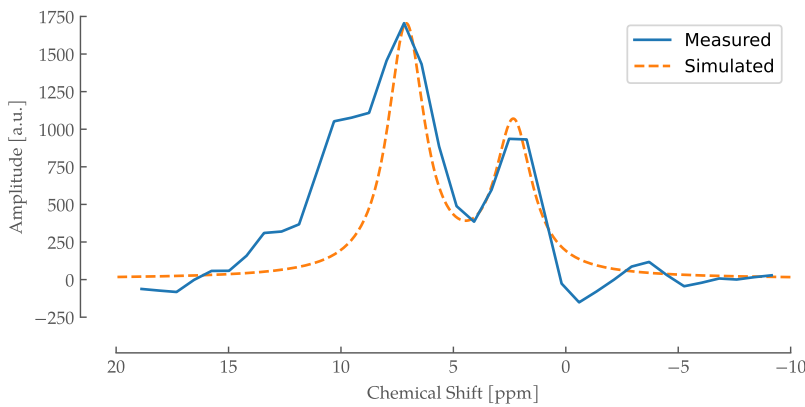


Figure 5.16: FID of Toluene. It was recorded under similar conditions as the water above. A simple $\frac{\pi}{2}$ -pulse of $9 \mu\text{s}$ with 1 W power at 25.0904 MHz was sent. After a delay of $25 \mu\text{s}$ the signal was recorded for 20 ms.

Figure 5.16 shows the FID received from the Toluene sample measured analogous to the FID of the water signal shown in Figure 5.2. The signal was recorded after a $9 \mu\text{s}$ pulse and a $25 \mu\text{s}$ delay. As opposed to the water signal in Figure 5.2 the toluene signal in Figure 5.16 is not a simple decaying sine wave anymore, but a superposition of multiple frequencies. The signal, however, decays in a similar time frame as before. Again, the first points should be discarded as an erroneous output of the CIC filters. Additionally, the signal could be extrapolated backwards by the delay time to reduce the sinc baseline distortions stemming from the window effect.

The superposition of multiple frequencies can be easily analysed in the Fourier spectrum shown in [Figure 5.17](#). As is common practice in NMR spectra, the scale here is in ppm relative to the B_0 field of 25 MHz — 1 ppm = 2.5 Hz — and not an absolute frequency. The zero point for the simulation was set by MestReNova by definition to the resonance frequency of **TMS**⁹. The measured signal has been manually shifted as the spectrometer has no locking functionality yet. Lastly, the x-axis is inverted for historical reasons.



9: The resonance frequency of the ^1H nuclei in **TMS** is relatively low so that a lot of signals are assigned a positive chemical shift. It is an accepted international standard.

Figure 5.17: FFT of Toluene measurement and simulation over a ppm scale. The blue data line was obtained through a Fourier transformation of the signal in [Figure 5.16](#). It was manually shifted by 170 Hz as there is no locking yet. The orange signal was created using MestReNova 14.3.3 simulating a spectra of Toluene at a B_0 field of 25 MHz, a peak width of 50 Hz and scaled to match the measurement scale.

The simulated dashed orange line in [Figure 5.17](#) shows the expected signal for Toluene in a B_0 field of 25 MHz while the blue line is the manually cropped and shifted measurement data. The expected peak at 2 ppm of the Methyl group is easily distinguishable from the peak of the Benzene ring at \approx 7.2 ppm. The artefacts already seen in the water signal can be observed here as well. The peak broadening now is on the left side of the peak — due to the inverted x-axis and the sinc artefact from the windowing and the erroneous first points are clearly visible on the right side of the graph.

This page intentionally left blank.

6

CONCLUSION

I choose a lazy person to do a hard job. Because a lazy person will find an easy way to do it.

— Bill Gates

[Chapter 2](#) briefly introduced the basic concepts needed to understand the electronics and chemistry of the spectrometer. [Chapter 3](#) then looked at the different parts of it in detail, whereas [Chapter 4](#) described the usage of the whole system. Finally, [Chapter 5](#) described and discussed the experimental results obtained with the designed system.

An affordable low-field low-cost easy-to-use and easy-to-build NMR spectrometer was designed, built characterised and tested.

Immediate next steps include the completion of the shimming system and more iterations on the probe. Tuning and matching should be possible from outside the magnet for easier and quicker operation in addition to shielding to remove the RF noise. The improvement points mentioned at the end of each sections should be addressed.

The main functions separated into individual parts allow for easy reconfiguration and experimentation during the early stages of the project. A final design could later integrate them on a single [PCB](#), reducing cost further as well as noise due to a shorter path and raising signal power due to fewer reflections and impedance mismatches.

Looking especially towards its application in the Global South, the temperature behaviour and stability of the system need first to be characterized and then possibly compensated through isolation cooling and/or heating.

With the recently increasing focus on low-field low-cost magnetic resonance work leveraging the higher capabilities and lower costs of modern electronics — especially in the [SDR](#) domain — a joint effort and interface would be highly advantageous as well. Some homebrew NMR console control software solutions exist and have been mentioned before. A lot of them are rudimentary and not compatible with each other. While software solutions for analysing spectra exist, processing spectra can be cumbersome not only due to the various

file formats but also due to the focus of existing tools on commercial systems which often provide proprietary processing options.

There is still a lot to be done before *magnETHical* is ready for deployment. It lays the groundwork for further optimization, integration and exploration. It is the beginning of a great new quest!

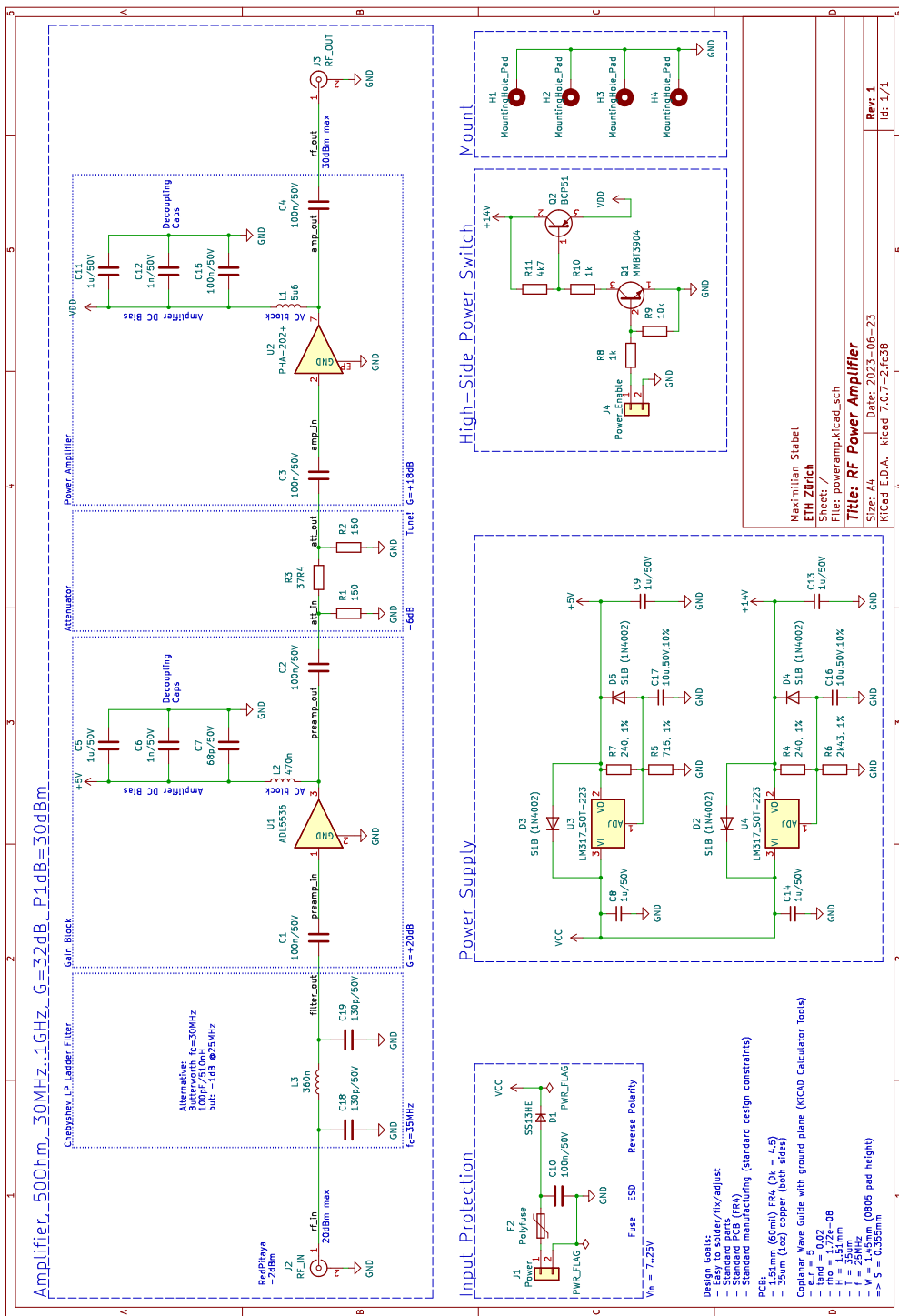
APPENDIX

This page intentionally left blank.

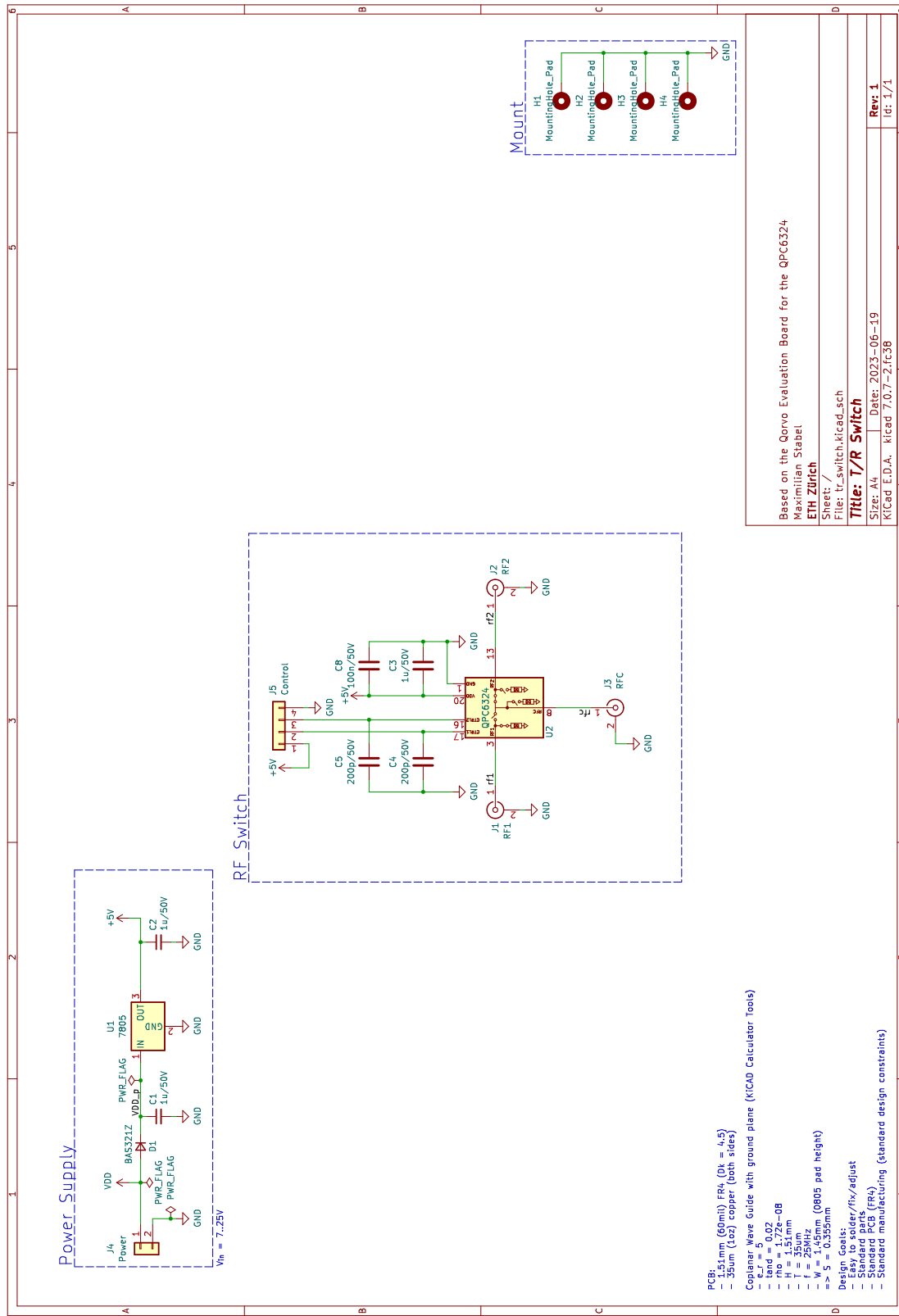
SCHEMATICS

A

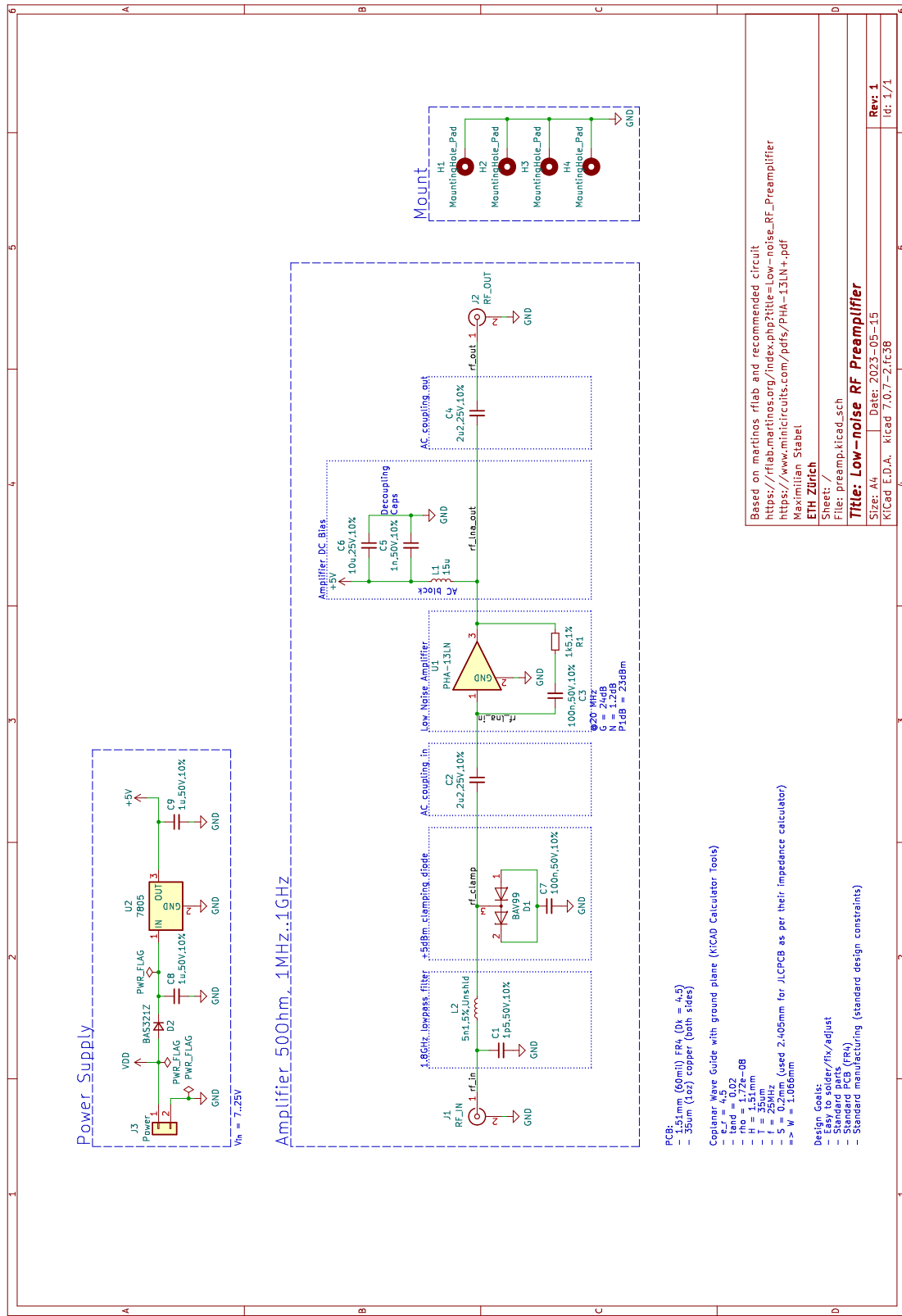
A.1 THE POWER AMPLIFIER



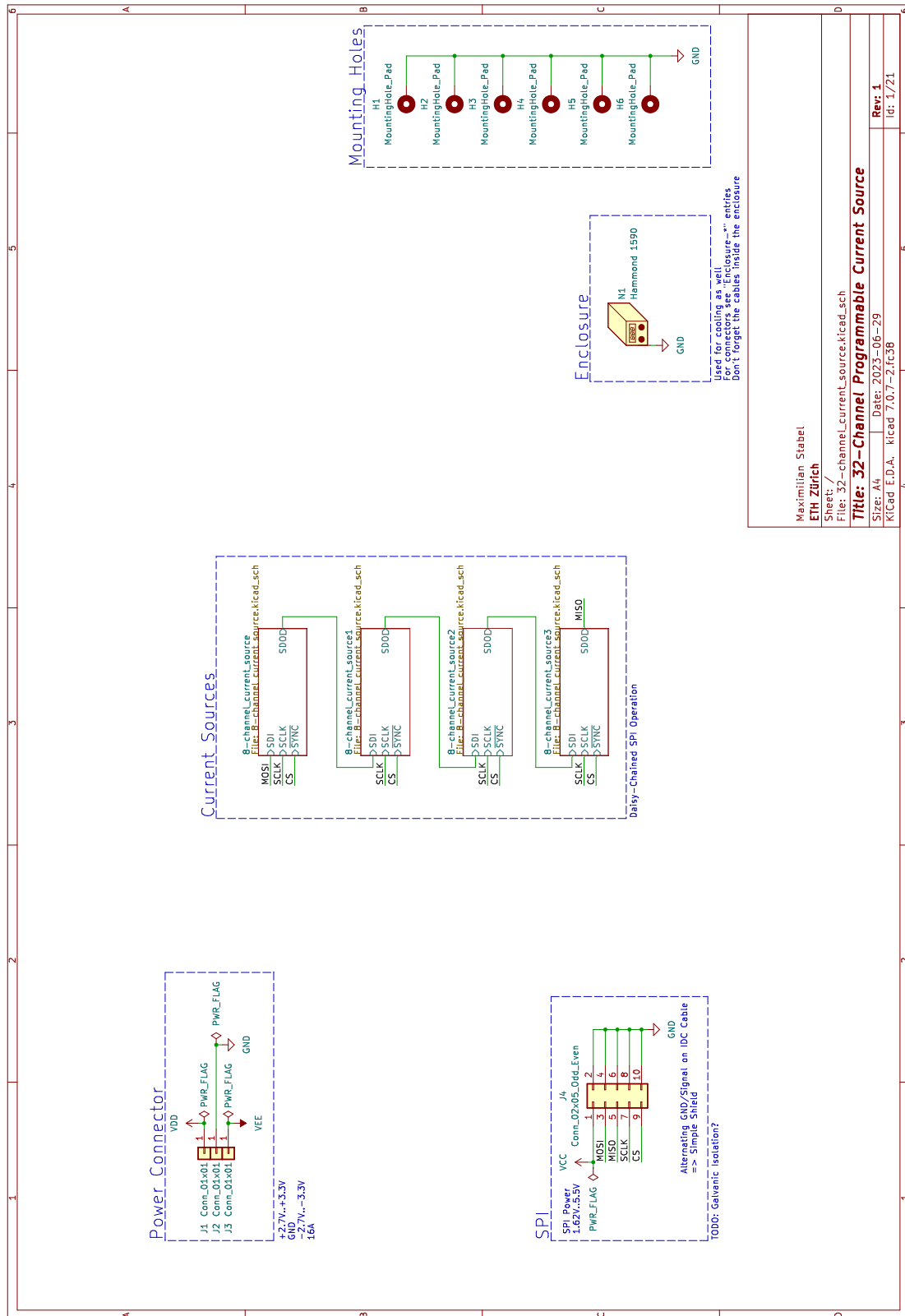
A.2 THE SWITCH

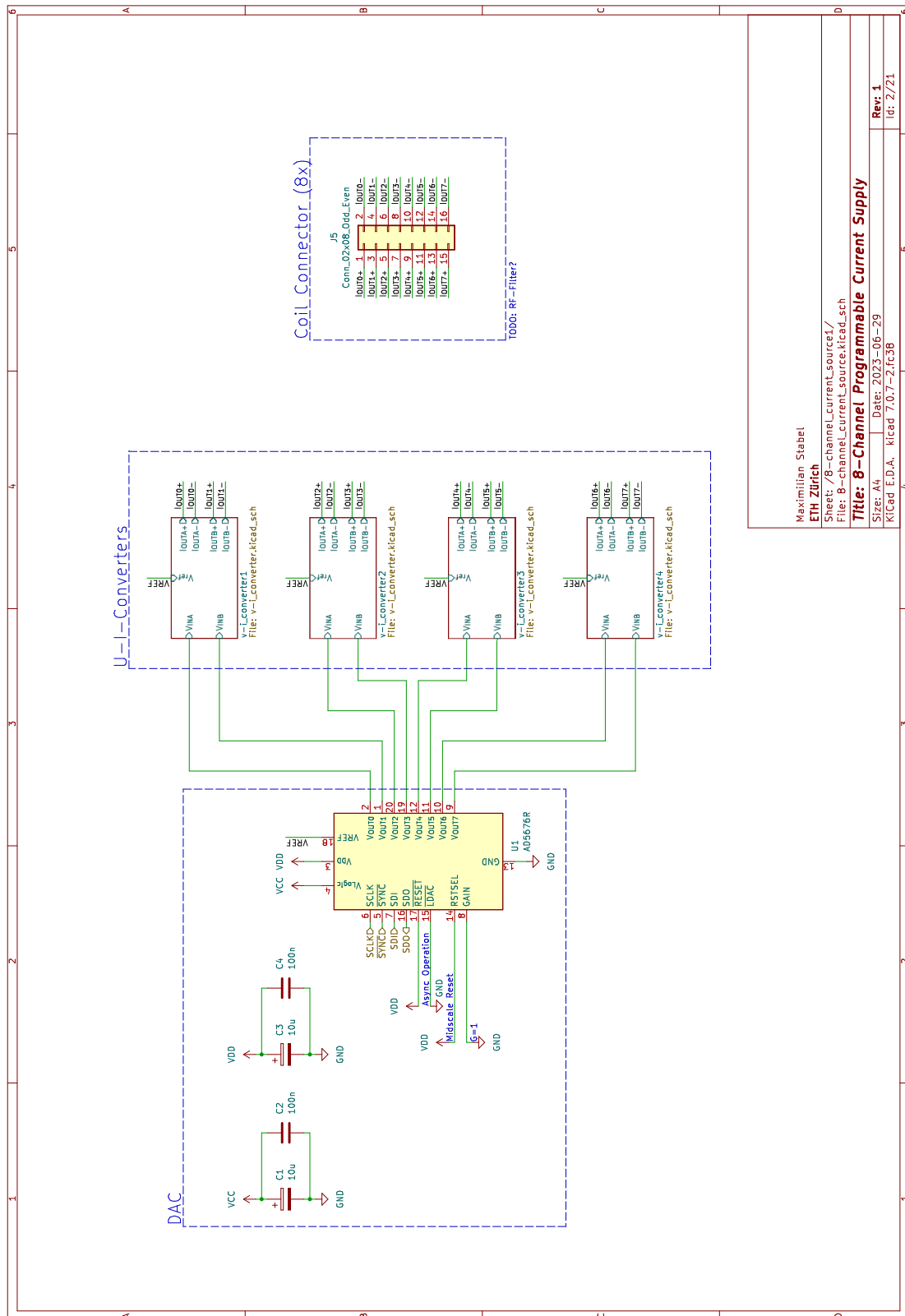


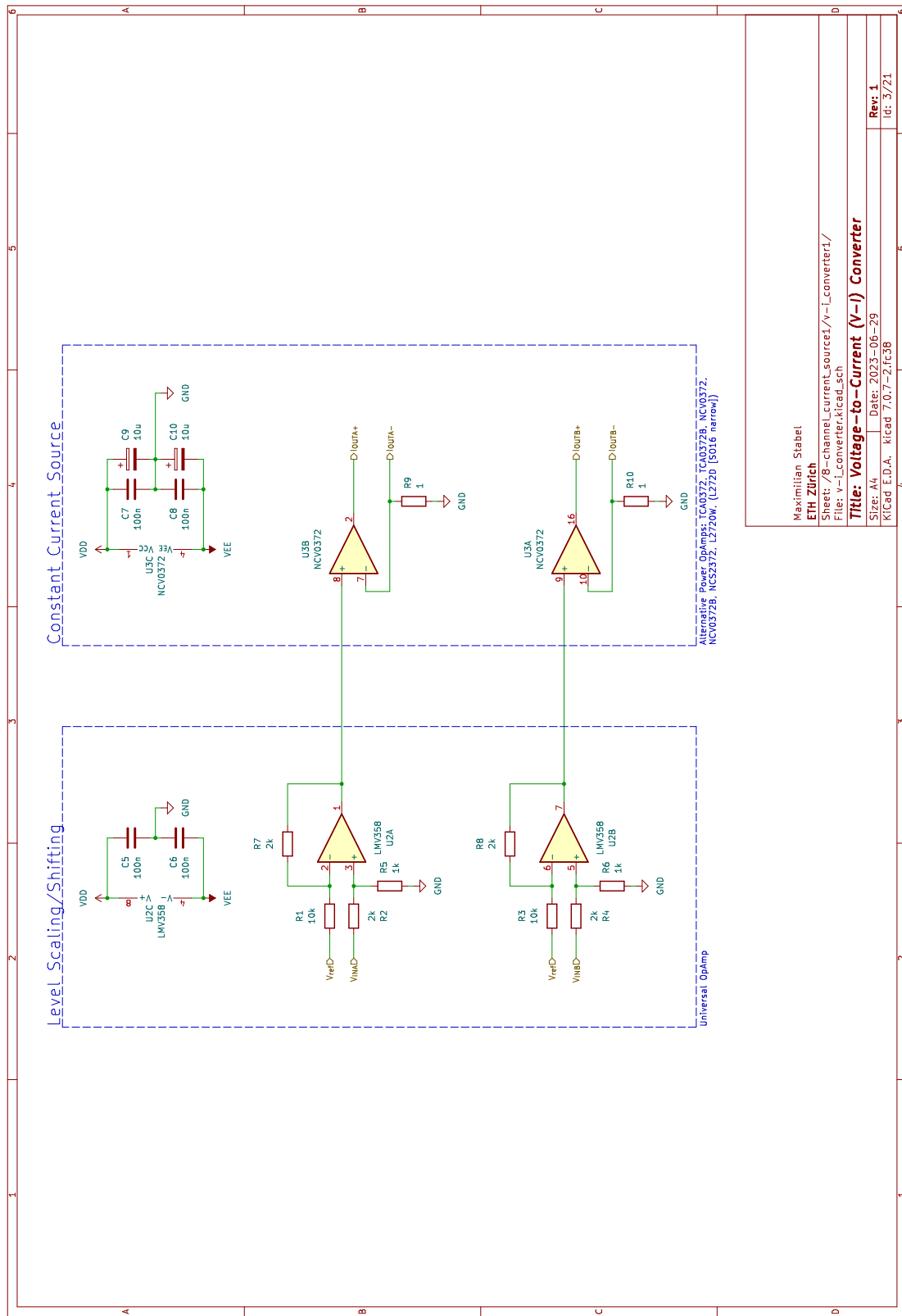
A.3 THE LOW NOISE AMPLIFIER



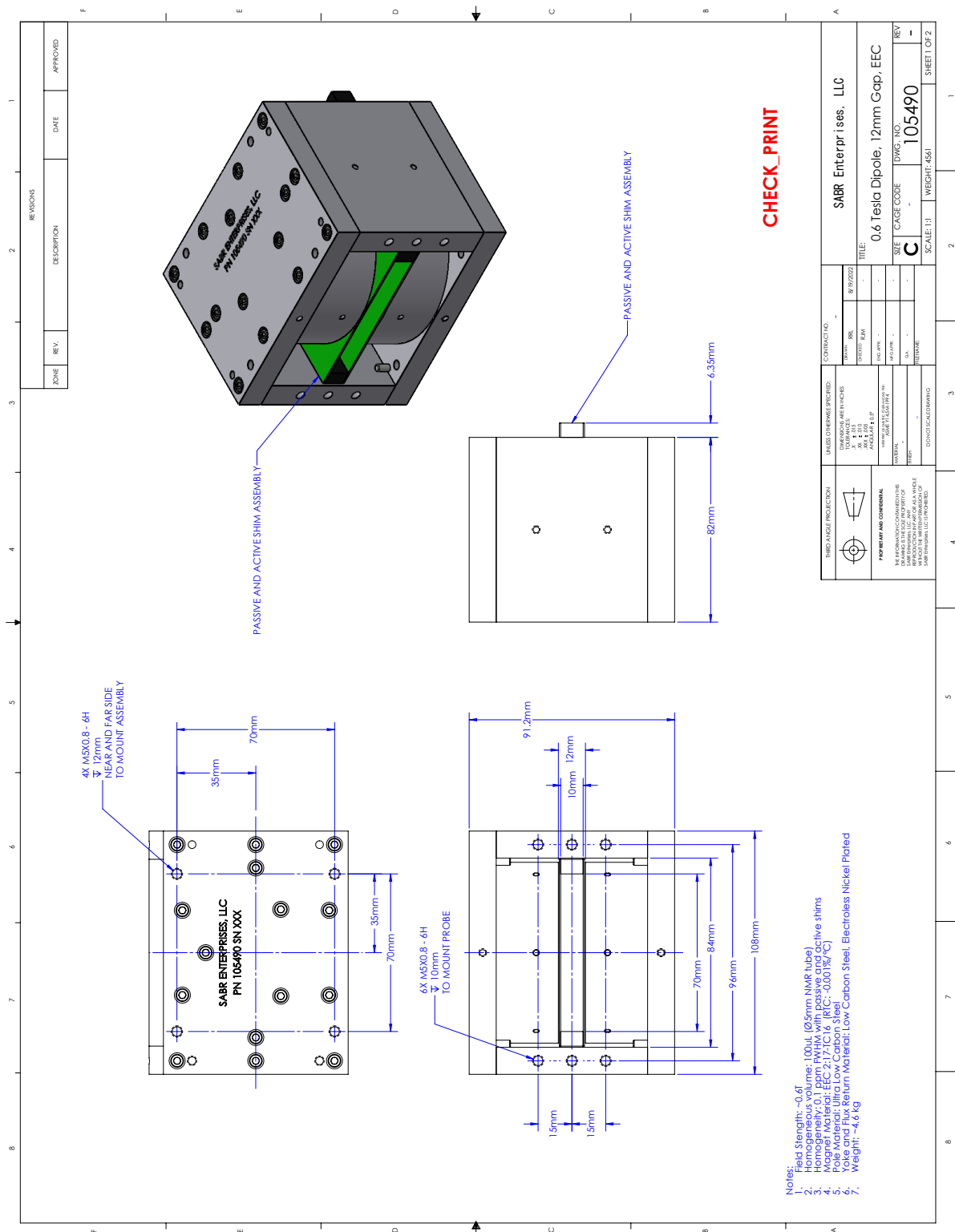
A.4 THE 32-CHANNEL CURRENT SOURCE







A.5 THE MAGNET



This page intentionally left blank.

LISTS OF PARTS

B

Below are the complete part lists for the schematics above — also called **BOMs**. A lot of standard parts are available from many different manufacturers, the given **Manufacturer Part Number (MPN)** in these cases are only one of many possible options. For example most of the RLC parts, the linear power supplies (7850, LM317, ...) and the pin headers — among others.

As customary in a lot of designs, the comma dot has often been replaced by the SI-Prefix for the given value or the variable name in case of no prefix. For example, 4k7 for a resistor is equivalent to $4.7\text{ k}\Omega$. Equivalently, a 5u6 capacitor has a value of $5.6\text{ }\mu\text{F}$. If there is no prefix, the symbol is sometimes used, for example, 37R4 is equal to a 37.4Ω resistor. This is usually done for better readability and less ambiguity — especially on bad prints where the point can easily vanish.

B.1 THE POWER AMPLIFIER

Qty	Reference(s)	Value	MPN
6	C ₁ , C ₂ , C ₃ , C ₄ , C ₁₀ , C ₁₅	100n,50V,10%	Co805C104J5RACTU
6	C ₅ , C ₁₁ , C ₈ , C ₉ , C ₁₃ , C ₁₄	1u,50V,10%	CL21B105KBFNNNG
2	C ₆ , C ₁₂	1n,50V,10%	08055C102KAT2A
1	C ₇	68p,50V	08055A680JAT2A
2	C ₁₆ , C ₁₇	10u,50V,10%	GRM21BR61H106KE43L
2	C ₁₈ , C ₁₉	130p/50V	GRM2165C1H131JA01D
1	D ₁	SS13HE,Schottky,30V,1A	SS13HE
4	D ₂ , D ₃ , D ₄ , D ₅	S1B (1N4002)	S1B-13-F
1	F ₂	PTC fuse,6V,0.75A,0.2s,40mΩ	0805L075SL
1	J ₁	Power	68491-102HLF
1	J ₂	RF_IN	142-0701-851
1	J ₃	RF_OUT	142-0701-851
1	J ₄	Power_Enable	68491-102HLF
1	L ₁	5u6	CC453232-5R6KL
1	L ₂	470n	L-15FR47JV4E
1	L ₃	360n,5%,RF	36502AR36JTDG
1	Q ₁	MMBT3904	MMBT3904-7-F
1	Q ₂	BCP51	BCP51,115
2	R ₁ , R ₂	150	ACo805FR-07150RL
1	R ₃	37R4	CRo805-FX-37R4ELF
2	R ₄ , R ₇	240, 1%	RCo805FR-07240RL
1	R ₅	715, 1%	RTo805FRE07715RL
1	R ₆	2k43, 1%	ERJ-6ENF2431V
2	R ₈ , R ₁₀	1k	1623131-1
1	R ₉	10k	CRCW080510KoFKEAC
1	R ₁₁	4k7	ACo805FR-074K7L
1	U ₁	ADL5536	ADL5536ARKZ-R7
1	U ₂	PHA-202+	PHA-202+
2	U ₃ , U ₄	LM317_SOT-223	LM317MQDCYR

B.2 THE SWITCH

Qty	Reference(s)	Value	MPN
3	C ₁ , C ₂ , C ₃	1u/50V	CL21B105KBFNNNG
2	C ₄ , C ₅	200p/50V	C0805C201K5HACTU
1	C ₈	100n/50V	C0805C104J5RACTU
1	D ₁	BAS321Z	BAS321Z
1	J ₁	RF ₁	142-0701-851
1	J ₂	RF ₂	142-0701-851
1	J ₃	RFC	142-0701-851
1	J ₄	2x,2.54mm pitch,pin header	68491-102HLF
1	J ₅	4x,2.54mm pitch,pin header	69190-104HLF
1	U ₁	7805	UA78M05IDCYR
1	U ₂	QPC6324	QPC6324

B.3 THE LOW NOISE AMPLIFIER

Qty	Reference(s)	Value	MPN
1	C1	1p5,50V,10%	CC0805BRNPO9BN1R5
2	C2, C4	2u2,25V,10%	CL21A225KAFNNNG
2	C3, C7	100n,50V,10%	CL21B104KBCNNNC
1	C5	1n,50V,10%	CL21B102KBANFNC
1	C6	10u,25V,10%	CL21A106KAYNNNG
2	C8, C9	1u,50V,10%	CL21B105KBFNNNG
1	D1	BAV99	BAV99
1	D2	BAS321Z	BAS321Z
1	J1	RF_IN	142-0701-851
1	J2	RF_OUT	142-0701-851
1	J3	Power	68491-102HLF
1	L1	15u	CV201210-150K
1	L2	5n1,5%,Unshld	0805HT-5N1TJLC
1	R1	1k5,1%	RT0805FRE101K5L
1	U1	PHA-13LN	PHA-13LN+
1	U2	7805	UA78M05IDCYR

B.4 THE 32-CHANNEL CURRENT SOURCE

Qty	Reference(s)	Value	MPN
40	C ₁ , C ₃ , C ₉ , C ₁₀ , C ₁₅ , C ₁₆ , C ₂₁ , C ₂₂ , C ₂₇ , C ₂₈ , C ₂₉ , C ₃₁ , C ₃₇ , C ₃₈ , C ₄₃ , C ₄₄ , C ₄₉ , C ₅₀ , C ₅₅ , C ₅₆ , C ₅₇ , C ₅₉ , C ₆₅ , C ₆₆ , C ₇₁ , C ₇₂ , C ₇₇ , C ₇₈ , C ₈₃ , C ₈₄ , C ₈₅ , C ₈₇ , C ₉₃ , C ₉₄ , C ₉₉ , C ₁₀₀ , C ₁₀₅ , C ₁₀₆ , C ₁₁₁ , C ₁₁₂	10u, tantalum	TMCP1A106KTRF
72	C ₂ , C ₄ , C ₅ , C ₆ , C ₇ , C ₈ , C ₁₁ , C ₁₂ , C ₁₃ , C ₁₄ , C ₁₇ , C ₁₈ , C ₁₉ , C ₂₀ , C ₂₃ , C ₂₄ , C ₂₅ , C ₂₆ , C ₃₀ , C ₃₂ , C ₃₃ , C ₃₄ , C ₃₅ , C ₃₆ , C ₃₉ , C ₄₀ , C ₄₁ , C ₄₂ , C ₄₅ , C ₄₆ , C ₄₇ , C ₄₈ , C ₅₁ , C ₅₂ , C ₅₃ , C ₅₄ , C ₅₈ , C ₆₀ , C ₆₁ , C ₆₂ , C ₆₃ , C ₆₄ , C ₆₇ , C ₆₈ , C ₆₉ , C ₇₀ , C ₇₃ , C ₇₄ , C ₇₅ , C ₇₆ , C ₇₉ , C ₈₀ , C ₈₁ , C ₈₂ , C ₈₆ , C ₈₈ , C ₈₉ , C ₉₀ , C ₉₁ , C ₉₂ , C ₉₅ , C ₉₆ , C ₉₇ , C ₉₈ , C ₁₀₁ , C ₁₀₂ , C ₁₀₃ , C ₁₀₄ , C ₁₀₇ , C ₁₀₈ , C ₁₀₉ , C ₁₁₀	100n, ceramic, low ESR, low ESI	0805ZD104KAT2A
2	J ₁ , J ₃	Red, banana power plug, enclosure	6091
1	J ₂	Black, banana power plug, enclosure	6092
1	J ₄	10pos, 2row, DIN41651, 72454-010LF 2.54mm pitch, idc	
4	J ₅ , J ₆ , J ₇ , J ₈	16pos, 2row, DIN41651, 72454-016LF 2.54mm pitch, idc	
1	N ₁	Enclosure, Hammond 1590	1590Z150
32	R ₁ , R ₃ , R ₁₁ , R ₁₃ , R ₂₁ , R ₂₃ , R ₃₁ , R ₃₃ , R ₄₁ , R ₄₃ , R ₅₁ , R ₅₃ , R ₆₁ , R ₆₃ , R ₇₁ , R ₇₃ , R ₈₁ , R ₈₃ , R ₉₁ , R ₉₃ , R ₁₀₁ , R ₁₀₃ , R ₁₁₁ , R ₁₁₃ , R ₁₂₁ , R ₁₂₃ , R ₁₃₁ , R ₁₃₃ , R ₁₄₁ , R ₁₄₃ , R ₁₅₁ , R ₁₅₃	10k	RT0805FRE1310KL

64	R ₂ , R ₄ , R ₇ , R ₈ , R ₁₂ , R ₁₄ , R ₁₇ , R ₁₈ , R ₂₂ , R ₂₄ , R ₂₇ , R ₂₈ , R ₃₂ , R ₃₄ , R ₃₇ , R ₃₈ , R ₄₂ , R ₄₄ , R ₄₇ , R ₄₈ , R ₅₂ , R ₅₄ , R ₅₇ , R ₅₈ , R ₆₂ , R ₆₄ , R ₆₇ , R ₆₈ , R ₇₂ , R ₇₄ , R ₇₇ , R ₇₈ , R ₈₂ , R ₈₄ , R ₈₇ , R ₈₈ , R ₉₂ , R ₉₄ , R ₉₇ , R ₉₈ , R ₁₀₂ , R ₁₀₄ , R ₁₀₇ , R ₁₀₈ , R ₁₁₂ , R ₁₁₄ , R ₁₁₇ , R ₁₁₈ , R ₁₂₂ , R ₁₂₄ , R ₁₂₇ , R ₁₂₈ , R ₁₃₂ , R ₁₃₄ , R ₁₃₇ , R ₁₃₈ , R ₁₄₂ , R ₁₄₄ , R ₁₄₇ , R ₁₄₈ , R ₁₅₂ , R ₁₅₄ , R ₁₅₇ , R ₁₅₈	2k	RT0805FRE072KL
32	R ₅ , R ₆ , R ₁₅ , R ₁₆ , R ₂₅ , R ₂₆ , R ₃₅ , R ₃₆ , R ₄₅ , R ₄₆ , R ₅₅ , R ₅₆ , R ₆₅ , R ₆₆ , R ₇₅ , R ₇₆ , R ₈₅ , R ₈₆ , R ₉₅ , R ₉₆ , R ₁₀₅ , R ₁₀₆ , R ₁₁₅ , R ₁₁₆ , R ₁₂₅ , R ₁₂₆ , R ₁₃₅ , R ₁₃₆ , R ₁₄₅ , R ₁₄₆ , R ₁₅₅ , R ₁₅₆	1k	RT0805FRE071KL
32	R ₉ , R ₁₀ , R ₁₉ , R ₂₀ , R ₂₉ , R ₃₀ , R ₃₉ , R ₄₀ , R ₄₉ , R ₅₀ , R ₅₉ , R ₆₀ , R ₆₉ , R ₇₀ , R ₇₉ , R ₈₀ , R ₈₉ , R ₉₀ , R ₉₉ , R ₁₀₀ , R ₁₀₉ , R ₁₁₀ , R ₁₁₉ , R ₁₂₀ , R ₁₂₉ , R ₁₃₀ , R ₁₃₉ , R ₁₄₀ , R ₁₄₉ , R ₁₅₀ , R ₁₅₉ , R ₁₆₀	1, precision, current sense	ERJ-6DQF1RoV
4	U ₁ , U ₁₀ , U ₁₉ , U ₂₈	AD5676R	AD5676RBRUZ
16	U ₂ , U ₄ , U ₆ , U ₈ , U ₁₁ , U ₁₃ , U ₁₅ , U ₁₇ , U ₂₀ , U ₂₂ , U ₂₄ , U ₂₆ , U ₂₉ , U ₃₁ , U ₃₃ , U ₃₅	LMV358	LMV358IDR
16	U ₃ , U ₅ , U ₇ , U ₉ , U ₁₂ , U ₁₄ , U ₁₆ , U ₁₈ , U ₂₁ , U ₂₃ , U ₂₅ , U ₂₇ , U ₃₀ , U ₃₂ , U ₃₄ , U ₃₆	NCV0372	NCV0372BDWR2G
1	-	10pos, 2row, DIN41651, 2.54mm pitch, ids, enclosure	4610-6000
4	-	16pos, 2row, DIN41651, 2.54mm pitch, idc, enclosure	4616-6000
1	-	10pos, 2row, DIN41651, 2.54mm pitch, ids, cable	71600-310LF
4	-	16pos, 2row, DIN41651, 2.54mm pitch, idc, cable	71600-316LF

BIBLIOGRAPHY

References in citation order.

- [1] P. Zeeman, "On the influence of magnetism on the nature of the light emitted by a substance," *Verslagen en Mededeelingen der Kon. Academie van Wetenschappen, Afd. Natuurkunde*, vol. 5, pp. 181–184, Jan. 1, 1896 (cited on page 1).
- [2] I. I. Rabi, J. R. Zacharias, S. Millman, and P. Kusch, "A New Method of Measuring Nuclear Magnetic Moment," *Physical Review*, vol. 53, no. 4, pp. 318–318, Feb. 15, 1938. doi: [10.1103/PhysRev.53.318](https://doi.org/10.1103/PhysRev.53.318) (cited on page 1).
- [3] F. Bloch, W. W. Hansen, and M. Packard, "The Nuclear Induction Experiment," *Physical Review*, vol. 70, no. 7-8, pp. 474–485, Oct. 1, 1946. doi: [10.1103/PhysRev.70.474](https://doi.org/10.1103/PhysRev.70.474) (cited on page 1).
- [4] E. M. Purcell, H. C. Torrey, and R. V. Pound, "Resonance Absorption by Nuclear Magnetic Moments in a Solid," *Physical Review*, vol. 69, no. 1-2, pp. 37–38, Jan. 1, 1946. doi: [10.1103/PhysRev.69.37](https://doi.org/10.1103/PhysRev.69.37) (cited on page 1).
- [5] R. R. Ernst and W. A. Anderson, "Application of Fourier Transform Spectroscopy to Magnetic Resonance," *Review of Scientific Instruments*, vol. 37, pp. 93–102, Jan. 1966. doi: [10.1063/1.1719961](https://doi.org/10.1063/1.1719961) (cited on page 1).
- [6] M. W. Nielsen and J. P. Andersen, "Global citation inequality is on the rise," *Proceedings of the National Academy of Sciences*, vol. 118, no. 7, e2012208118, Feb. 16, 2021. doi: [10.1073/pnas.2012208118](https://doi.org/10.1073/pnas.2012208118) (cited on page 1).
- [7] M. H. Levitt, *Spin Dynamics: Basics of Nuclear Magnetic Resonance*, 2nd ed. Chichester, England ; Hoboken, NJ: John Wiley & Sons, Apr. 21, 2008, 714 pp. (cited on page 3).
- [8] E. Fukushima, *Experimental Pulse NMR: A Nuts and Bolts Approach*. Boca Raton: CRC Press, Jan. 21, 1981, 556 pp. (cited on page 3).
- [9] U. Tietze, C. Schenk, and E. Gamm, *Halbleiter-Schaltungstechnik*, 16., erweiterte und aktualisierte Auflage. Berlin [Heidelberg]: Springer Vieweg, 2019, 1793 pp. (cited on pages 3, 26, 29).
- [10] P. Horowitz and W. Hill, *The Art of Electronics*, Third edition, 19th printing with corrections. New York: Cambridge University Press, 2022, 1230 pp. (cited on page 3).
- [11] K. Takeda, "A highly integrated FPGA-based nuclear magnetic resonance spectrometer," *Review of Scientific Instruments*, vol. 78, no. 3, p. 033 103, Mar. 1, 2007. doi: [10.1063/1.2712940](https://doi.org/10.1063/1.2712940). (visited on 09/30/2023) (cited on page 9).
- [12] V. Negnevitsky, Y. Vives-Gilabert, J. M. Algarín, *et al.*, "MaRCoS, an open-source electronic control system for low-field MRI," *Journal of Magnetic Resonance*, vol. 350, p. 107 424, May 2023. doi: [10.1016/j.jmr.2023.107424](https://doi.org/10.1016/j.jmr.2023.107424) (cited on page 11).
- [13] A. Louis-Joseph and P. Lesot, "Designing and building a low-cost portable FT-NMR spectrometer in 2019: A modern challenge," *Comptes Rendus. Chimie*, vol. 22, pp. 695–711, Sep. 2019. doi: [10.1016/j.crci.2019.07.001](https://doi.org/10.1016/j.crci.2019.07.001). (visited on 09/21/2023) (cited on pages 13, 14).

- [14] J. Mispelter, M. Lupu, and A. Briguet, *NMR Probeheads for Biophysical and Biomedical Experiments: Theoretical Principles and Practical Guidelines*, 2nd ed. IMPERIAL COLLEGE PRESS, Jul. 2015. (visited on 09/21/2023) (cited on pages 13, 19).
- [15] H.-Y. Chen, Y. Kim, P. Nath, and C. Hilty, “An ultra-low cost NMR device with arbitrary pulse programming,” *Journal of Magnetic Resonance*, vol. 255, pp. 100–105, Jun. 1, 2015. doi: [10.1016/j.jmr.2015.02.011](https://doi.org/10.1016/j.jmr.2015.02.011). (visited on 09/22/2023) (cited on page 14).
- [16] I. J. Lowe and C. E. Tarr, “A fast recovery probe and receiver for pulsed nuclear magnetic resonance spectroscopy,” *Journal of Physics E: Scientific Instruments*, vol. 1, no. 3, pp. 320–322, Mar. 1968. doi: [10.1088/0022-3735/1/3/312](https://doi.org/10.1088/0022-3735/1/3/312). (visited on 09/05/2023) (cited on page 16).
- [17] B. Blümich, S. Haber-Pohlmeier, and W. Zia, “Compact NMR,” in *Compact NMR*, De Gruyter, Jan. 31, 2014. doi: [10.1515/9783110266719](https://doi.org/10.1515/9783110266719). (visited on 09/27/2023) (cited on page 29).
- [18] H. Raich and P. Blümller, “Design and construction of a dipolar Halbach array with a homogeneous field from identical bar magnets: NMR Mandhalas: Design of a Dipolar Halbach Array,” *Concepts in Magnetic Resonance Part B: Magnetic Resonance Engineering*, no. 1, pp. 16–25, Oct. 2004. doi: [10.1002/cmr.b.20018](https://doi.org/10.1002/cmr.b.20018). (visited on 09/27/2023) (cited on page 29).
- [19] E. Danieli, J. Perlo, B. Blümich, and F. Casanova, “Small Magnets for Portable NMR Spectrometers,” *Angewandte Chemie International Edition*, vol. 49, no. 24, pp. 4133–4135, 2010. doi: [10.1002/anie.201000221](https://doi.org/10.1002/anie.201000221). (visited on 09/27/2023) (cited on page 30).
- [20] A. J. Parker, W. Zia, C. W. G. Rehorn, and B. Blümich, “Shimming Halbach magnets utilizing genetic algorithms to profit from material imperfections,” *Journal of Magnetic Resonance*, vol. 265, pp. 83–89, Apr. 1, 2016. doi: [10.1016/j.jmr.2016.01.014](https://doi.org/10.1016/j.jmr.2016.01.014). (visited on 09/27/2023) (cited on page 30).
- [21] J. Wang, X. Jiang, Z. Hu, *et al.*, “Design and Shimming Method of Low Length-to-Interdiameter Ratio Halbach Magnet,” *IEEE Transactions on Instrumentation and Measurement*, vol. 71, pp. 1–10, 2022. doi: [10.1109/TIM.2022.3199233](https://doi.org/10.1109/TIM.2022.3199233). (visited on 09/27/2023) (cited on page 30).
- [22] J. J. Helmus and C. P. Jaroniec, “Nmrglue: An open source Python package for the analysis of multidimensional NMR data,” *Journal of Biomolecular NMR*, vol. 55, no. 4, pp. 355–367, Apr. 1, 2013. doi: [10.1007/s10858-013-9718-x](https://doi.org/10.1007/s10858-013-9718-x). (visited on 08/21/2023) (cited on page 30).
- [23] F. Delaglio, S. Grzesiek, G. W. Vuister, G. Zhu, J. Pfeifer, and A. Bax, “NMRPipe: A multidimensional spectral processing system based on UNIX pipes,” *Journal of biomolecular NMR*, vol. 6, no. 3, pp. 277–293, Nov. 1995. doi: [10.1007/BF00197809](https://doi.org/10.1007/BF00197809) (cited on page 30).
- [24] D. Schober, D. Jacob, M. Wilson, *et al.*, “nmrML: A Community Supported Open Data Standard for the Description, Storage, and Exchange of NMR Data,” *Analytical Chemistry*, vol. 90, no. 1, pp. 649–656, Jan. 2, 2018. doi: [10.1021/acs.analchem.7b02795](https://doi.org/10.1021/acs.analchem.7b02795). (visited on 09/29/2023) (cited on page 30).

- [25] R. S. McDonald and P. A. Wilks, "JCAMP-DX: A Standard Form for Exchange of Infrared Spectra in Computer Readable Form," *Applied Spectroscopy*, vol. 42, no. 1, pp. 151–162, Jan. 1, 1988. doi: [10.1366/0003702884428734](https://doi.org/10.1366/0003702884428734). (visited on 09/29/2023) (cited on page 30).
- [26] R. C. Martin, *Clean Code: A Handbook of Agile Software Craftsmanship*, 1st edition. Upper Saddle River, NJ Munich: Pearson, Aug. 1, 2008, 464 pp. (cited on page 31).
- [27] V. W. Miner and W. W. Conover, *Shimming Ain't Magic - The Shimming of High Resolution NMR Magnets*, Acorn NMR Inc., 1997. [Online]. Available: https://web.mit.edu/8.13/www/pdf_files/shimming.pdf (visited on 09/24/2023) (cited on page 38).
- [28] J. Keeler, *Understanding NMR Spectroscopy*, 2nd ed. Chichester, U.K: John Wiley and Sons, 2010, 511 pp. (cited on page 41).
- [29] M. Suzuki and I. Suzuki, "Lecture Note on Senior Laboratory Spin echo method in pulsed nuclear magnetic resonance (NMR)," Mar. 4, 2011 (cited on page 42).

This page intentionally left blank.

SPECIAL TERMS

A

AC Alternating Current. [18](#)
ADC Analogue-to-ditigal converter. [xi, 24, 28](#)
API Application Programming Interface. [30, 34](#)

B

BOM Bill Of Material. [59](#)

C

CHF Swiss Francs. [xiii, 9](#)
CIC Cascaded Integrator-Comb. [10, 38, 44](#)
CLI Command-Line Interface. [30](#)
CONTINOUS WAVE NUCLEAR MAGNETIC RESONANCE SPECTROSCOPY is an [Nuclear Magnetic Resonance spectroscopy](#) experiment performed by slowly varying the excitation frequency and observing the resonance behaviour of nuclei inside the sample. [4, 69](#)
CW-NMR [Continous Wave Nuclear Magnetic Resonance spectroscopy](#). [4](#)

D

DAC Digital-to-analog converter. [xi, 27, 28](#)
DC direct current. [14, 16, 18, 24](#)
DHCP Dynamic Host Configuration Protocol. [33](#)

F

FET Field-Effect Transistor. [xi, 18, 29](#)
FFT Fast Fourier Transform. [xii, 45](#)
FID Free Induction Decay. [xi, xii, 37, 38, 41–44](#)

FOURIER TRANSFORM NUCLEAR MAGNETIC RESONANCE SPECTROSCOPY Instead of slowly varying the frequency as in [Continous Wave Nuclear Magnetic Resonance spectroscopy](#), a single pulse of a given length with a fixed frequency is sent. According to Fourier's theory, this "smears" the frequency and excites nuclei with different resonant frequencies simultaneously. [1, 69](#)

FPGA Field-Programmable Gate Array. [9, 11, 30, 71](#)

FREE SOFTWARE is software available with a license that allows everyone to not only run but also look at, change and redistribute it freely – i.e. it is distributed with the source code. It is thus different from freeware and especially proprietary software. The FSF puts it as: "Think of 'free' as in 'free speech' not as in 'free beer'.". [69, 70](#)

FT-NMR Fourier Transform Nuclear Magnetic Resonance spectroscopy. [1, 4](#)

G

GNU is an extensive collection of [Free Software](#) developed within the GNU Project which can be used to form a complete operating system – the most famous one known as Linux. Its goal is to give computer users freedom and control in their use of computers by developing software under the copyleft [GPL](#), that guarantees access to the source code of the software. [70](#)

GPIO General-Purpose Input/Output. [18](#)

GPL [GNU](#) General Public License. [69](#)

GWN Gaussian White Noise. [39](#)

I

IC Integrated Circuit. [26](#)

IID Independent and Identically Distributed. [39](#)

IP Internet Protocol. [32](#), [33](#)

K

[KiCAD](#) is an open source [Free Software](#) schematic capture and electronic design software endorsed by CERN for open hardware development. [x](#), [xi](#), [24](#), [28](#)

L

[LCR METER](#) is an electronic test equipment to measure inductance (L), capacitance (C) and resistance (R). [7](#), [10](#)

LED Light Emitting Diode. [26](#)

[LINUX](#) [GNU/Linux](#). [32](#), [33](#)

LNA low-noise amplifier. [9](#), [24](#), [32](#)

M

[MAGNETIC RESONANCE](#) is a phenomenon where atomic nuclei in a strong constant magnetic field, excited by a second oscillating magnetic field of correct frequency resonate and emit a corresponding electromagnetic signal. [1](#), [70](#)

[MARCoS](#) MAgnetic Resonance COntrol System. [11](#), [30](#)

[MMIC](#) Monolithic Microwave Integrated Circuit. [ix](#), [14](#), [15](#)

[MPN](#) Manufacturer Part Number. [59–63](#)

[MR](#) [Magnetic Resonance](#). [1](#)

[MRI](#) Magnetic Resonance Imaging. [1](#)

N

[NMR](#) [Nuclear Magnetic Resonance spectroscopy](#). [v](#), [xi](#), [xii](#), [2](#), [3](#), [9](#), [32](#), [37](#), [44](#)

[NUCLEAR MAGNETIC RESONANCE SPECTROSCOPY](#) is a spectroscopic technique to observe shifts in magnetic field strengths in atomic nuclei. Or in simpler terms a [Hidden Force Looking Machine](#). [v](#), [2](#), [69](#), [70](#)

O

[OPAMP](#) Operational Amplifier. [x](#), [xi](#), [27–29](#)

P

PA power amplifier. [32](#)

[PCB](#) Printed Circuit Board. [ix–xi](#), [15](#), [18](#), [19](#), [24–26](#), [28](#), [47](#)

[PIP](#) pip Install Packages. [xiii](#), [34](#)

[PYTHON](#) is a high-level interpreted general-purpose cross-platform programming language designed by Guido van Rossum. It focuses on readability and ease of use with a “batteries included” approach. The [Zen of Python](#) states among others: “There should be one – and preferably only one – obvious way to do it”. (For the seasoned “Pythoneer”: Try “`import` this” and “`import` antigravity”). [xiii](#), [31–34](#)

R

REDPITAYA is a company producing credit card sized computers including an **FPGA** which run open-source software (the hardware itself is *not* open-source). In the context of the thesis, this refers to the specific board used – a RedPitaya **SDRlab 122-16** based on a Xilinx **SoC** (Zynq 7020 with Dual ARM Cortex A9, 122.88 MHz clock and 50Ω terminated **RF** inputs). [71](#)

RF radio frequency. [ix-xi](#), [3](#), [11](#), [14-20](#), [22](#), [24](#), [31](#), [37](#), [71](#)

RMS Root Mean Square. [39](#)

RP **RedPitaya**. [11](#), [32](#), [33](#)

S

SDR Software Defined Radio. [47](#)

SMA **SubMiniature version A connector**. [xi](#), [31](#), [32](#)

SNR Signal-to-Noise Ratio. [39](#)

SoC System on a Chip. [71](#)

SPDT Single Pole, Double Throw. [x](#), [18](#), [19](#)

SPI Serial Peripheral Interface. [x](#), [xi](#), [27](#), [28](#)

SSH Secure Shell. [33](#)

STD Standard Deviation. [39](#)

SUBMINIATURE VERSION A CONNECTOR is a common small coaxial RF connector with a screw-on connection designed for high frequencies (tens of GHz) often used for WiFi antennas and handheld radio devices among others. [71](#)

T

T/R Transmit/Receive. [x](#), [17](#), [19](#)

TMS Tetramethylsilane. [4](#), [45](#)

U

USB Universal Serial Bus. [28](#)

V

VAT Value Added Tax. [xiii](#), [9](#)

VNA Vector Network Analyser. [7](#), [21](#)

This page intentionally left blank.

DECLARATION OF ORIGINALITY

I hereby confirm that I am the sole author of the written work here enclosed and that I have compiled it in my own words. Parts excepted are corrections of form and content by the supervisor.

Title of work: Building a 25 MHz NMR Spectrometer

Authored by: Maximilian Stabel

With my signature, I confirm that

- I have committed none of the forms of plagiarism described in the “[Citation etiquette](#)” information sheet.
- I have documented all methods, data and processes truthfully.
- I have not manipulated any data.
- I have mentioned all persons who were significant facilitators of the work.

I am aware that the work may be screened electronically for plagiarism.

Place, date

Maximilian Stabel